Chapter 8

Vacuum System

8.1 Introduction

The vacuum system for the SuperKEKB[1][2] [3] [4] has been designed based on various experiences obtained during the operation of the KEKB [5][6][7][8][9][10][11][12][13], while also introducing leading-edge concepts[14]. The main parameters related to the vacuum system are listed in Table 8.1 [1]. The first major issue of the vacuum system comes from the high beam currents, that is, 3.6 A for 4 GeV positron ring (Low Energy Ring, LER) and 2.6 A for 7 GeV electron ring (High Energy Ring, HER). The synchrotron radiation (SR) power and the photon flux are consequently high, and the resultant heat and gas loads are also large. The second issue comes from the high bunch current (1.44 $\sim$ 1.04 mA per bunch) and the short bunch length (5 $\sim$ 6 mm). Higher order modes (HOM) are likely to be excited as a result, and the beam impedance of various vacuum components needs to be minimized to keep the stored beams stable and also to avoid excess heating of components. The third and probably most serious issue is the electron cloud effect (ECE) in the positron ring, LER [15][16][17]. More rigorous countermeasures than before are required to reduce the electron density in the beam pipe. Otherwise, a single-bunch instability may be excited and the luminosity will deteriorate considerably. Various research and development had been performed using the KEKB in order to overcome these issues for the SuperKEKB [14]. The existing monitor and control system [18] are reused as much as possible, but the antiquated systems will be replaced by the latest ones. The infrastructures, such as the water cooling system and the compressed air system, will be also reused after partial upgrades. The following is an outline of the vacuum system design for mainly the main ring (MR) of the SuperKEKB, but is especially concentrated on the LER where the most of vacuum components are replaced to new ones. The design for the Interaction Region (IR) and for the Damping Ring (DR) of the positron beam will be

presented in other section.

8.2 Beam pipe

8.2.1 Cross sections

General

One ring consists of approximately 1000 beam pipes, which are each 2 - 6 m in length. The new beam pipe for the SuperKEKB basically consists of a circular beam channel and two rectangular antechambers on each side (we call this an antechamber structure) [19][20][21][22]. Typical cross sections of a beam pipe with antechamber structure is shown in Fig. 8.1 (a)-(c). The beam goes through a beam channel at the center, and usually the synchrotron radiation (SR) passes through an antechamber located outside the ring (we call it an SR channel) and hits the side wall of the antechamber. The SR is irradiated along the sidewall. A photon-stop scheme, where the SR is locally irradiated, will not be realized due to a high concentrated power on the photon stop. In arc sections, the antechamber located inside the ring is used as a pump chamber (we call it a pump channel). The pump channel is connected to the beam channel through a screen with many holes (4 mm in diameter and 5 mm in thickness) for pumping and also for RF shielding (see Sec.5). In some sections where the SR hit both sides such as a wiggler section, the SR passes through both antechambers, and there is no screen and pump channel. The pumps are located at the bottom of antechambers in this case. The pumping port should also have a screen with many holes with a diameter of 5 mm for RF shielding (3 - 5 mm in thickness). For non-antechamber type beam pipes, such as the reused beam pipes of HER, the pumping ports are located at the bottom of beam channel [5][6]. In principle, a cooling channel is at outside of the sidewall of each beam pipe to absorb the heat from the SR. For beam pipes with antechamber structure, another cooling channel is also prepared at inside of the ring to make the temperature uniform in a beam pipe as shown in Fig. 8.1 (a)-(c). The first advantage of the antechamber structure is that a low beam impedance can be realized [23]. For the cross-section as presented in Fig. 8.1 (a)-(c), the electric field accompanied by a bunch is orders of magnitude smaller in the antechamber than in the beam channel, due to the narrow height of the antechamber. Therefore, the pumping ports in an antechamber or the screen in a pump channel have a small beam impedance. SR masks, which are usually placed downstream of a beam pipe to protect the following flanges and bellows chambers from SR, also have little effect on the beam if placed in the antechamber. Naturally, the cross-section of the beam pipe is effectively kept uniform. The second

	LER (positron)	HER (electron)	Unit
Beam energy	4.0	7.0	GeV
Beam current	3.6	2.6	A
Circumference	3016		m
Number of bunches	2500		
Bunch current	1.44	1.06	mA
Bunch length	6.0	5.0	mm
$\varepsilon_x/\varepsilon_y$	3.2/8.64	4.6/11.5	nm/pm
β_x^*/β_y^*	32/0.27	25/0.3	mm
ν_s	-0.0244	-0.0280	
Crossing angle	83		mrad
Luminosity	8×10^{35}		$cm^{-2}s^{-1}$
Bending radius (Arc)	74.68 (arc)	105.98 (arc)	m
Beam pipe material (Arc)	Al-alloy (arc) OFC (wiggler)	OFC (arc), OFC (wiggler)	
Cross section of beam pipe (Arc)	ϕ 90 + Antechambers	Racetrack (50×104) ϕ 50 + Antechambers	
Main pumps (Arc)	NEG (strip)	NEG (strip + cartridge)	
Total Power of SR[a,b|	1.1 (arc:2200 m) 6.3 (wiggler:300 m)	5.2 (arc: 2200 m) 1.1 (wiggler:100 m)	MW
Critical Energy of SR	1.9 (arc) 9.2 (wiggler)	7.2 (arc) 17 (wiggler)	keV
Max. SR power line density	2.6 (arc) 13 (wiggler)	7.7 (arc) 9 (wiggler)	kWm^{-1}
Avg. SR power line density	0.56 (arc)	2.6 (arc)	kWm^{-1}
Total photon flux	1.2×10^{22} (arc) 1.4×10^{22} (wiggler)	1.5×10^{22} (arc) 1.3×10^{21} (wiggler)	photons s^{-1}
Avg. photon flux line density	5.5×10^{18}(arc) 4.7×10^{19}(wiggler)	6.8×10^{18}(arc) 1.3×10^{19}(wiggler)	photons $s^{-1}m^{-1}$
Linear pumping speed	0.1 (arc)	0.06 (arc)	$m^3s^{-1}m^{-1}$
Ave. pressure with beam[c)	$\sim 10^{-7}$		Pa
Ave. base pressure	$\sim 10^{-8}$		Pa
Static desorption rate	$< 10^{-8}$		Pa $m^3s^{-1}m^{-2}$

a) Synchrotron Radiation

b) Wiggler parameters

LER: $\rho = 15.48\text{m}, \theta = 11.2\text{mrad}$, #672

HER: $\rho = 45.52\text{m}, \theta = 7.6\text{mrad}$, #72

c) ρ of 1×10^{-6} molecules photon^{-1} is assumed.

Table 8.1: Main parameters and important values related to the vacuum system of SuperKEKB.

advantage of the antechamber structure is that the power density of SR can be reduced because of its vertical and horizontal spread. That is because the irradiated point of SR on the side wall is far from the point of SR emission, that is, a point on the beam orbit inside of a bending magnet at upstream side. Generally, a beam pipe with a larger aperture is better for pumping, since the conductance increases with the aperture size. The impedance of the beam pipe is relatively small for large apertures. For example, the resistive wall impedance will decrease as increasing a distance between a beam and an inner wall (see Sec. 10) [24]. The aperture of beam pipes, however, is usually limited by the cores of magnets, such as bending magnets, quadrupole magnets, and sextupole magnets. Furthermore, an almost circular beam channel is preferable to minimize the incoherent tune shift due to the resistive wall (see also Sec. 10) [25][26]. The cross-section of the new beam pipe with antechamber structure fits the presently used magnets and makes the most of the limited space. For example, a half-height of antechambers is 7 mm for both LER and HER. An especially strict part of SR channel is in the sextupole magnet. The cores of a sextupole magnet are indicated in Fig. 8.1 (a). Grooves with a depth of about 2 mm should be cut on the corresponding part of SR channel to keep a clearance for the sextupole magnet. Decreasing the height of SR channel arise another problem as is discussed in the next section. In some sections in the ring, where special magnets or instruments are installed, the beam pipes will be simple pipes. Therefore, tapered structures are required at transitions where the antechamber type to the single-pipe type beam pipes are connected. Since the number of tapers is not so large, they will have small effect on the total impedance. Key points to be considered are a trapped mode that will be excited between adjacent tapered structure if placed closely, and the SR power density on the side wall of the beam pipes with tapers. Various types of bema pipes are used in the rings. Cross sections of beam pipes used in the SuperKEKB MR are summarized in Table 8.2.

LER

The antechamber structure for the positron ring, LER, helps to minimize photoelectron effects because the emission points of the photoelectrons, that is, the side walls of the antechamber, are far from the beam orbit [22]. As described later in Sec. 7, this is essential in in suppressing the electron cloud effect (ECE) [15][16] For LER, the typical diameter of the beam channel and the half width at the horizontal plane are 90 mm and 110 mm, respectively, as shown in Fig. 8.1 (a). The thickness of the beam pipe is 6 mm. Note that the microwave instability due to the impedance of the coherent synchrotron radiation (CSR), which can be sometimes important for a ring with a lower energy beam, requires a small aperture in order to utilize the shield effect of the beam

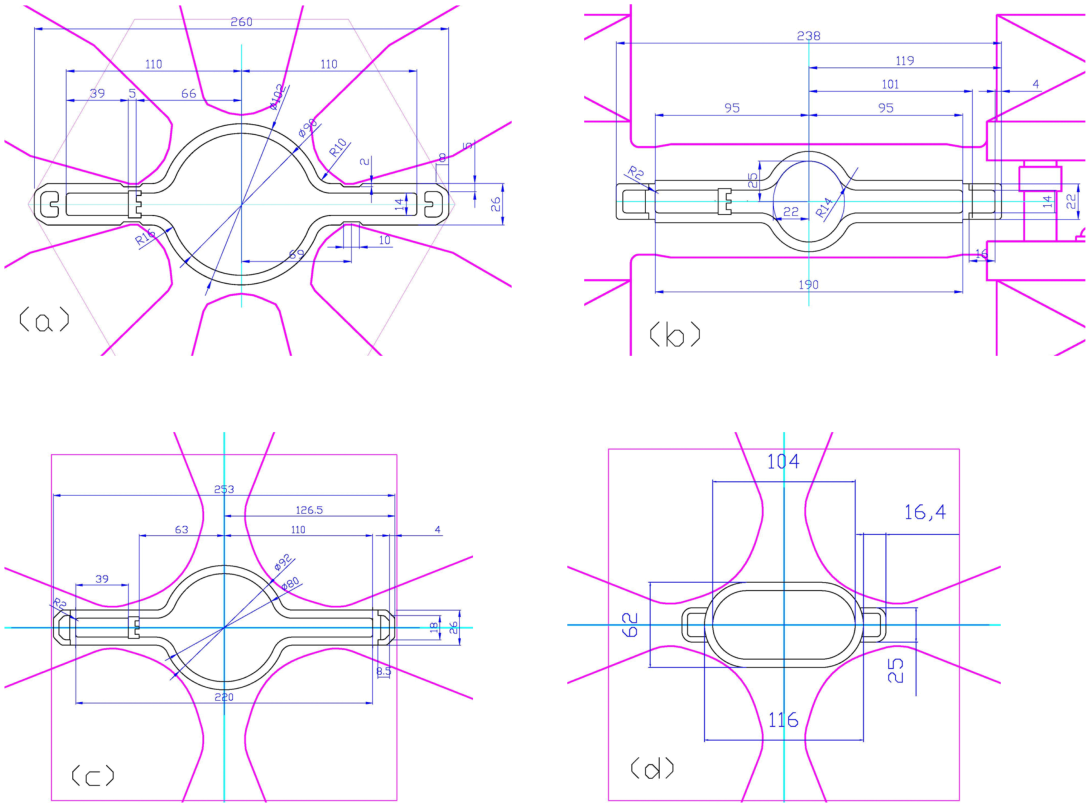

Figure 8.1: Typical cross sections of beam pipes for (a) LER with antechamber (f90x220) at arc sections in a sextupole magnet, (b) HER with antechambers (f50x190) at arc sections in a bending magnet, (c) HER with antechambers (f80x220) at straight sections in a quadrupole magnet and (d) HER with race-track shape (104x50) used in the KEKB at arc sections in a quadrupole magnet.

pipes [27][28]. The bunch lengthening due to the microwave instability including the CSR impedance, however, was found to be in a tolerable range even for the present aperture (see Sec. 10).

HER

For the arc section of the HER, most of beam pipes of the KEKB are simply reused in the SuperKEKB as it is. The cross section is a race-track shape with a half width of 52 mm and a half height of 25 mm [5], as shown in Fig. 8.1 (d). New beam pipes for the HER arc sections have an antechamber structure. The beam channel has an elliptical cross section with a long axis and short axis of 25 mm and 22 mm, respectively. The elliptical shape suppress the incoherent tune shift due to the wall current as explained in Sec. 10 [26]. The height of the beam channel was restricted by the aperture of the existing bending magnet of the KEKB. The half width of the beam pipe including the SR channel is 95 mm and the half height of the SR channel is 7 mm, as shown in Fig. 8.1 (b). The thickness of the beam pipe is 6 mm. The magnets in the straight sections of HER around the interaction region (IR) are newly manufactured, and the above geometrical restriction is released. The new beam pipes in that region has an antechamber structure with a radius of the beam channel of 40 mm and the half-width of 110 mm, as shown in Fig. 8.1 (c). The half-height of the SR channel is again 7 mm.

8.2.2 Height of SR channel

The half-height of SR channel of the antechamber is 7 mm for both LER and HER as described above. A small height of SR channel could relieve the spatial problem in sextupole magnets (see Fig. 8.1(a)-(c)). Actually, the half-height of 7 mm for the SR channel is enough to absorb SR within the SR channel, if the beam orbit is completely on the ideal plane. The vertical spreads of SR (γ^{-1}) for LER (4 GeV) and HER (7 GeV) are 0.13 mrad and 0.073 mard, respectively. On the other hand, the maximum distance between the adjacent bending magnets is about 20 m in the present lattice. The vertical half-height of SR at 20 m downstream side of a bending magnet are about 2.6 mm and 1.5 mm for LER and HER, respectively. Smaller SR channel height, therefore, seems available. A narrow SR channel will be also better for the LER since photoelectrons will be harder to come out from the SR channel. Usually, however, a raw beam orbit has a vertical deviation from its ideal one due to the setting and errors of magnets, and the results of beam tuning. SR from the vertically steered beam in a bending magnet may hit the beam channel instead of the sidewall of SR channel. In the Super KEKB, the raw beam orbit is kept flat as much as possible by using the skew

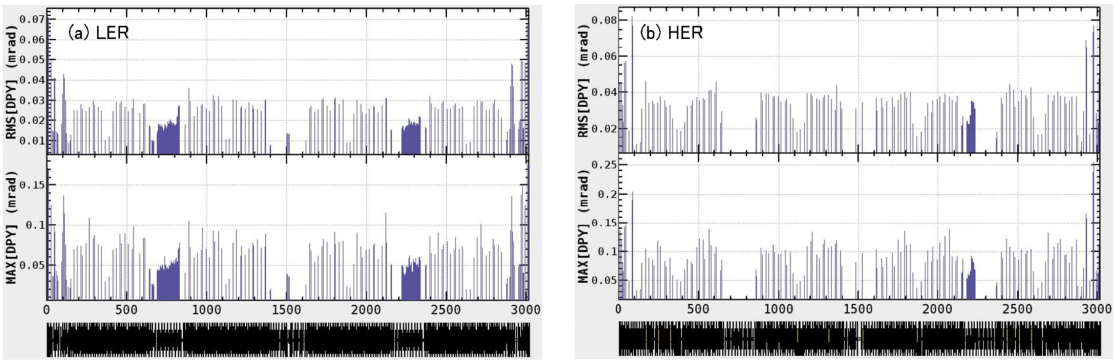

Figure 8.2: Distributions of RMS and Maximum vertical steering angles of circulating beams taking into account the alignment errors of magnets for (a) LER and (b) HER.

quadrupole component. But, in any way, the real orbit will have a deviation from an ideal one to some extent. Assuming that the vertical offset of raw beam orbit or that of beam pipe itself is 2 mm, the limit of angle of beam orbit are 0.12 mrad an 0.18 mrad for LER and HER, respectively, in order to confine the SR in the antechamber at 20 m downstream side. For reference, in the case of KEKB, the maximum deviation and angle of the beam orbit are 3 mm and 0.3 mrad for LER, and 2 mm and 0.2 mrad for HER, respectively [29]. Considering those values, the limit of the angle of the SuperKEKB seems well feasible. Actually, a tracking simulation indicated the RMS of the steering angles are less than 0.05 mrad and 0.08 mrad for LER and HER, respectively, as shown in Fig. 8.2 (a) and (b) [30]. Here the assumed setting (position and rotation) error of magnets (bending and quadrupole magnets) are 100 m and 100 rad, and that of the beam position monitor (BPM) are 75 m and 1 mrad, respectively.

8.2.3 SR power

The SR powers of LER and HER arc sections are 1.1 MW and 5.2 MW (see Table 8.1), respectively. The SR power of wiggler sections, on the other hand, are 6.3 MW and 1.1 MW for LER and HER, respectively. The SR is irradiated along the beam pipe as described above. The SR power line density along the LER and HER ring for a typical lattice cell are presented in Fig. 8.3 (a) and (b), respectively. The SR power line density at the wiggler section of LER and HER are also given in Fig. 8.3 (c) and (d), respectively. For the LER arc section, the maximum SR power line density (power density) is approximately 2.5 kW m^{-1} (2.4 W mm^{-2}) at a beam current of 3.6 A for a beam pipe with a half-width of 110 mm at just downstream side of a bending magnet. The average SR power line density is 0.56 kW m^{-1}. The SR power increases up to

Section	LER (positron)		HER (electron)	
	Cross section	Length [m]	Cross section	Length [m]
Arc[a),b)]	ϕ90×220 antechamber (Ha110)	2096	104×50 racetrack (Ha52)	2110
	ϕ90 circular [c)] (Ha45)	2096	ϕ50×190 antechamber [d)] (Ha95)	13
	[Aluminum alloy]		[OFHC]	
Interaction point	ϕ80 circular (Ha40)	30	ϕ80 circular (Ha40)	30
	[OFHC]		[OFHC]	
Local chromaticity correction	ϕ90×220 antechamber (Ha110)	240	ϕ80×220 antechamber (Ha110)	190
	ϕ90 circular (Ha45)	48	ϕ50×190 antechamber (Ha95)**	96
	[Aluminum alloy or OFHC]		[OFHC]	
Wiggler section and downstream	ϕ90×220 antechamber (Ha110)	351	ϕ90×220 antechamber (Ha110)	75
	[OFHC]		[OFHC]	
SR monitor	ϕ90×220-H24 antechamber [e)]	20	ϕ80×220 antechamber (Ha110)	9
	(Ha110)***		ϕ90×220-H24 antechamber	16
	[Aluminum alloy]		(Ha110)***	
			[Aluminum alloy or OFHC]	
Beam Injection	76×48 racetrack (Ha 38)	5	65×48 racetrack (Ha 32.5)	41
	[Aluminum alloy]		[Aluminum alloy]	
Beam Abort	122×50 racetrack (Ha 61)	6	122×50 racetrack (Ha 61)	9
	60×40 racetrack (Ha 30)	25	104×50 racetrack (Ha 52)	67
	[Aluminum alloy]		60×40 racetrack (Ha 30)	15
			[Aluminum alloy or OFHC]	
RF cavity	ϕ150 circular (Ha75) [OFHC]	142	ϕ150 circular (Ha75) [OFHC]	301
Beam monitor / feed back	ϕ110 circular (Ha55)	4	ϕ110 circular (Ha55)	8
	ϕ94 circular (Ha47)	32	ϕ104 circular (Ha52)	8
	ϕ64 circular (Ha32)	17	ϕ64 circular (Ha32)	28
	[Aluminum alloy or OFHC]		[Aluminum alloy or OFHC]	

a) Ha: Half aperture

b) OFHC: Oxygen Free Copper

c) In rotating sextupole magnets

d) Actually 50×44 elliptical

e) Full height of antechamber is 24 mm.

Table 8.2: Cross sections of beam pipes used in the ring.

approximately 7.7 kW m^{-1} (7.5 W mm^{-2}) at the SR mask with a height of 17 mm and a length of 180 mm, which blocks the SR to create shadows downstream. The wiggler section in the LER also required this antechamber structure to reduce the SR power density down to 13 kW m^{-1} (3 W mm^{-2}) at the end of wiggler region, where the bending radius of 15.48 m and the beam current of 3.6 A are assumed. The SR power increases up to approximately 45 kW m^{-1} (8 W mm^{-2}) at the SR mask with a height of 4 mm and a length of 370 mm. At the most downstream side of the wiggler section, that is, the entrance to the arc section from the straight wiggler section, the SR power concentrates to the pipe wall just in front of the beam. The SR power line density goes up to 77 kW m^{-1} (3.7 W mm^{-2}). The input power is huge although the power density is small. The special design is required for the SR masks in this region. In the case of HER arc sections, where a racetrack-shape beam pipe with a half aperture of 52 mm is used, the maximum SR power line density (power density) at an energy of 7 GeV and a beam current of 2.6 A is approximately 7.7 kW m^{-1} (16 W mm^{-2}), approximately the same as that of the KEKB HER (Energy of 8 GeV and a the design beam current of 1.4 A). This is because the increase in the beam current compensates for the reduction in the beam energy. The average SR power line density is 2.6 kW m^{-1}. The SR power increases up to approximately 27 kW m^{-1} (60 W mm^{-2}) at the SR mask with a height and a length of 10 mm and 140 mm, respectively. If a beam pipe with a half width of 95 mm is used for HER, the maximum SR power line density (power density) at an energy of 7 GeV and a beam current of 2.6 A is approximately 7.7 kW m^{-1} (12 W mm^{-2}). Compared to the case of racetrack-type described above, the SR line density is the same but the area density is reduced owing to the antechamber structure. The SR power density increases to 15 kW m^{-1} (24 W mm^{-2}) for the SR mask with a height and a length of 12 mm and 300 mm.

8.2.4 Material

Common materials for beam pipes of accelerators are stainless steel, copper and aluminum alloy [33]. Due to the high heat load from intense SR, the use of stainless steel for a part exposed to SR should be excluded in principle, since it has a low thermal conductivity. The high electrical resistivity, furthermore, is not preferable from the view point of the resistive-wall beam instability, and also of the heating due to Joule loss. For the LER arc sections, the power density is not so high as described in the previous section, and aluminum-alloy can be used from a view point of thermal strength. The machining and welding of aluminum-alloy are easier than copper. The TIG welding is available for aluminum alloy. We also had gotten various experiences on the aluminum beam pipe by the TRISTAN rings [32][33] as well as KEKB [5][6][7][8][9]. The beam

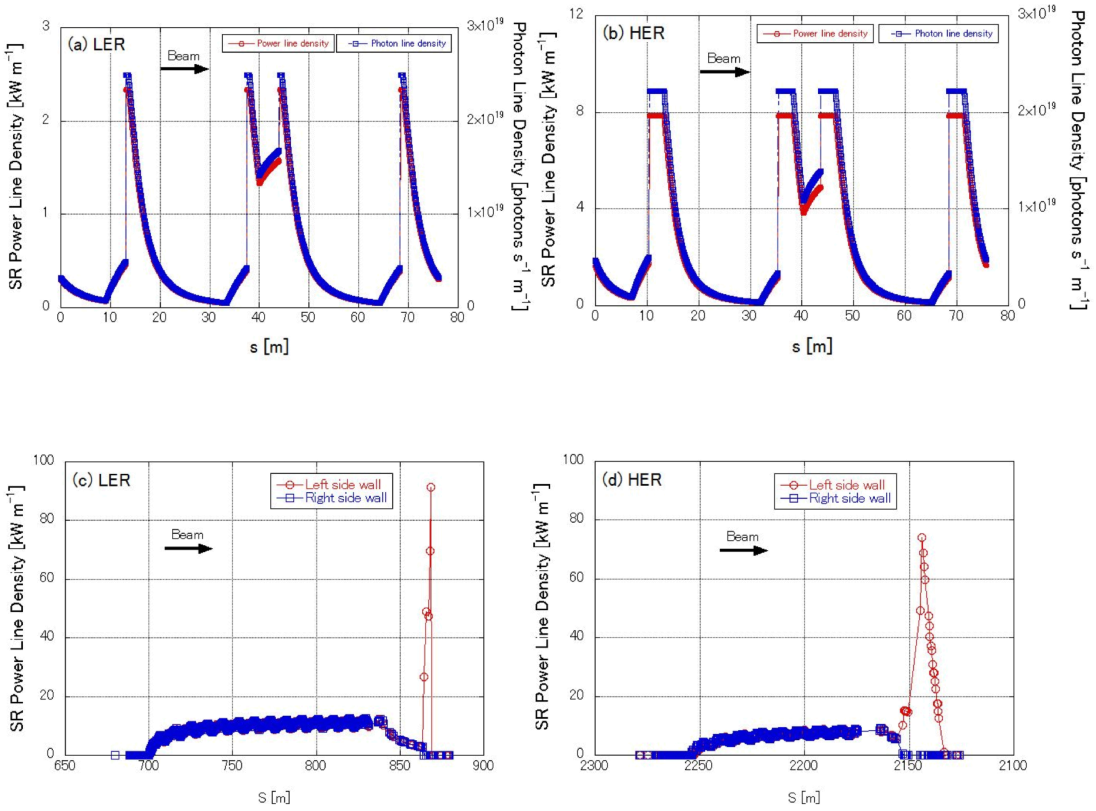

Figure 8.3: SR power line density and photon flux in a typical lattice cell for (a) LER and (b) HER at the design current. SR power line density in a wiggler section for (c) LER and (d) HER at the design current.

pipes for the LER arc section will be manufactured by aluminum alloy A6063-T6 or T5. The SR masks, where the SR power concentrate, the aluminum alloy of A5083 is used in some cases. Aluminum-alloy (A6063-T6 or T5) beam pipes with antechambers can be formed by an extrusion method. The penetrating radiation (X-ray, γ-ray and neutrons) caused by the beam loss, the SR and the bremsstrahlung can be a problem in using aluminum-alloy beam pipe. The critical energy of the SR of LER is 1.9 keV in the arc section (a beam energy of 4 GeV and a bending radius of 74.68 m). For the case of SuperKEKB, the integrated dose at outside of the beam pipe should be less than 1 MGy for 10 years in order to avoid the radiation damage of magnets or monitoring cables. Copper has a shorter radiation length, and has a better shielding property compared to aluminum-alloy. The simulation and the measurement, however, showed that the radiation level around the beam pipe of copper and aluminum-alloy is comparable for the thickness of 6 mm. A typical result of the simulation is presented in Fig. 8.4, where the dose at outside of the beam pipe are compared for aluminum and copper [34]. It was also found that the lead shielding is unnecessary even for aluminum-alloy at the arc section. High secondary electron yield (SEY) of aluminum surface is a serious problem for LER, since it enhance the electron density in the bam pipe and excite the electron cloud instability [35]. The beam pipe, therefore, will be coated with titanium-nitride (TiN) film to reduce the secondary electron yield [35][36]. The detailed will be described later (see Sec. 7). For the arc section of HER, on the other hand, copper should be the most suitable material for a beam pipe for its high thermal strength, high thermal conductivity, high radiation shielding and relatively low gas desorption rate. The critical energy of SR is 7.2 keV (a beam energy of 7 GeV and a bending radius of 105.98 m). The simulation showed that an aluminum beam pipe cannot be used due to the high radiation level around the beam pipe. No lead shielding is required for copper. Oxygen free copper (OFC, C1011) is a suitable material for its low gas desorption rate and good welding property. For the SR masks, copper-chrome alloy (CrCu, C18200) will be used in some cases. The antechamber-type beam pipe can be manufactured using the cold-drawn method. The cooling channels at both sides are welded separately by using an electron beam welding. Various experiences on copper beam pipes have been accumulated in the KEKB, such as a welding method and cleaning procedure [5][6][7][8][9]. For wiggler sections of LER and HER, where the SR power density at the side wall is much higher than that of arc sections, copper is a unique solution for the material of beam pipe. The SR masks are made of copper-chrome alloy (CrCu, C18200) that has higher mechanical strength. At the upstream side of interaction region (IR), where the background noise to the particle detector is a problem, the beam pipe is made of copper even for LER. The sources of

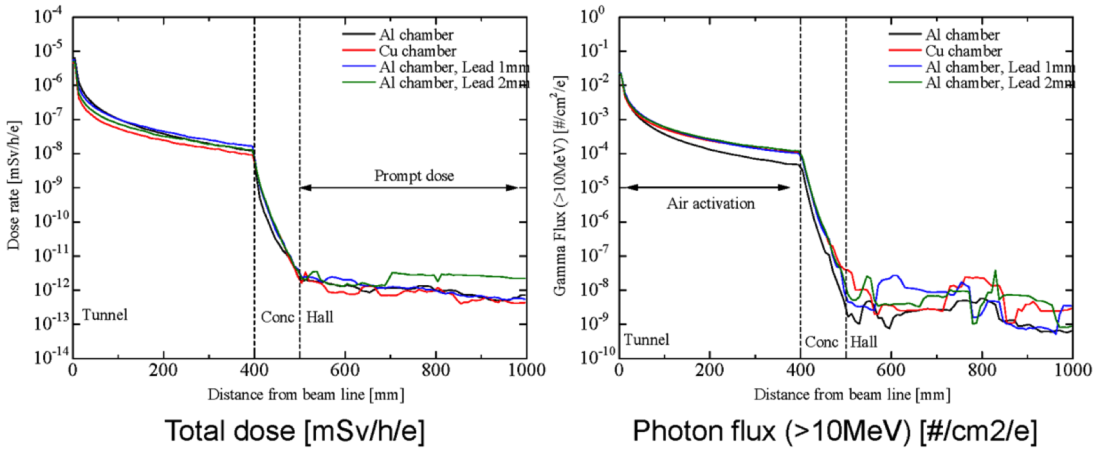

Figure 8.4: Dose rates outside beam pipes for aluminum beam pipe, copper beam pipe, aluminum beam pipe with 1 mm lead shielding and aluminum beam pipe with 2 mm lead shielding for LER, where the thickness of beam pipe is fixed to 6 mm. The annotations "Prompt does" and "Air activation" mean the dose rate outside concrete shielding and the gamma flux (>10 MeV) in the tunnel.

the noise are spent electrons, neutrons and gamma rays. Copper has higher radiation shielding property than aluminum-alloy. Aluminum-alloy beam pipes are also used for special and complex chambers, such as the beam pies for the beam injection region, the beam abort region, beam-size monitor region and so on. The working property and welding property are better for aluminum-alloy compared to copper. Several trial models of copper beam pipes with antechambers had been fabricated and installed into the KEKB LER to examine their properties using real beams [20][21][22]. The temperatures and vacuum pressures around the beam pipes were monitored during beam operation with a beam current up to 1.6 A (1585 bunches). The copper beam pipes were also installed into a wiggler section (∼30 m), together with bellows chambers and beam position monitors (BPM) described later. Although it was still within an acceptable range, the temperature of the stainless-steel flanges was high due to Joule heating of the stainless-steel surface. Copper-alloy flanges were developed in response to the result. The effect of the antechamber design on the number of photoelectrons was also studied, and a reduction in the number of photoelectrons by one or two orders of magnitude compared to a simple circular pipe was confirmed in a low beam-current region, although it was also found that the secondary electrons play a major role in a high beam-current region.

8.2.5 Mechanical property

Temperature distributions, deformations and stresses due to the irradiated SR and the atmospheric pressure (0.1 MPa) were calculated for various types of beam pipes described above. The calculations were three dimensional, and the heat convections to atmosphere and to cooling water were considered. Typical results for a beam pipe of the LER arc section are presented in Fig. 8.5 (a)-(d). The assumed material is A6063-T5. The vertical deformations due to the atmospheric pressure for with and without a screen are presented in Fig. 8.5 (a) and (b), respectively. The maximum deformations are 0.2 and 0.5 mm for the case with and without screen, respectively. The vertical deformation has no problem except for a beam position monitor (BPM) part. The BPM part, therefore, will be fabricated by a block and supported with ribs. Temperature distribution and the stress (Von mises stress) are presented in Fig. 8.5 (c) and (d), respectively. Here the input SR power of 7.5 W mm^{-2} for an irradiated width of 0.55 mm is assumed at the side wall of antechamber. The heat convection at the cooling channel is assumed to be 0.01 W mm^{-2}. The maximum temperature is approximately 100 °C at the irradiated point and the resultant thermal stress is 70 MPa. The temperature is well below the annealing temperature (approximately 250 °C). The stress is about 40 % of the yield strength (approximately 180 Pa). The beam pipe itself will withstand near 10^6 cycles with that stress [37].

8.2.6 Welding

The joint between aluminum alloys are basically TIG welding. The BPM block (A5083) and the flange (A2219) are butted after cutting the edge in V shape or mated to the extruded beam pipe (A6063) before welding. The material of welding filler is A4043. The welding is partial penetration and the thickness including the excess weld metal will be approximately 3 mm. The joint between copper alloys are basically the electron beam welding (EBW). The penetration thickness will be thicker than 3mm. The brazing is not allowable at the joint where the structural strength is required in order to avoid annealing of the material. The welding between stainless steels is also basically TIG welding. Aluminum alloy and copper alloy, and aluminum alloy and stainless steel will be joined by the hot isostatic pressing (HIP) method or explosive bonding. The thickness at the joint should be sufficiently thick to avoid leakage. Copper alloy and stainless steel will be joined by HIP or brazing. The mechanical and thermal stress is likely to be concentrated in the joint part. Special cares should be paid to the joint between the BPM blocks or the flanges, which have rigid structure, and the extruded beam pipe, which is relatively soft, in handling the beam pipe. The

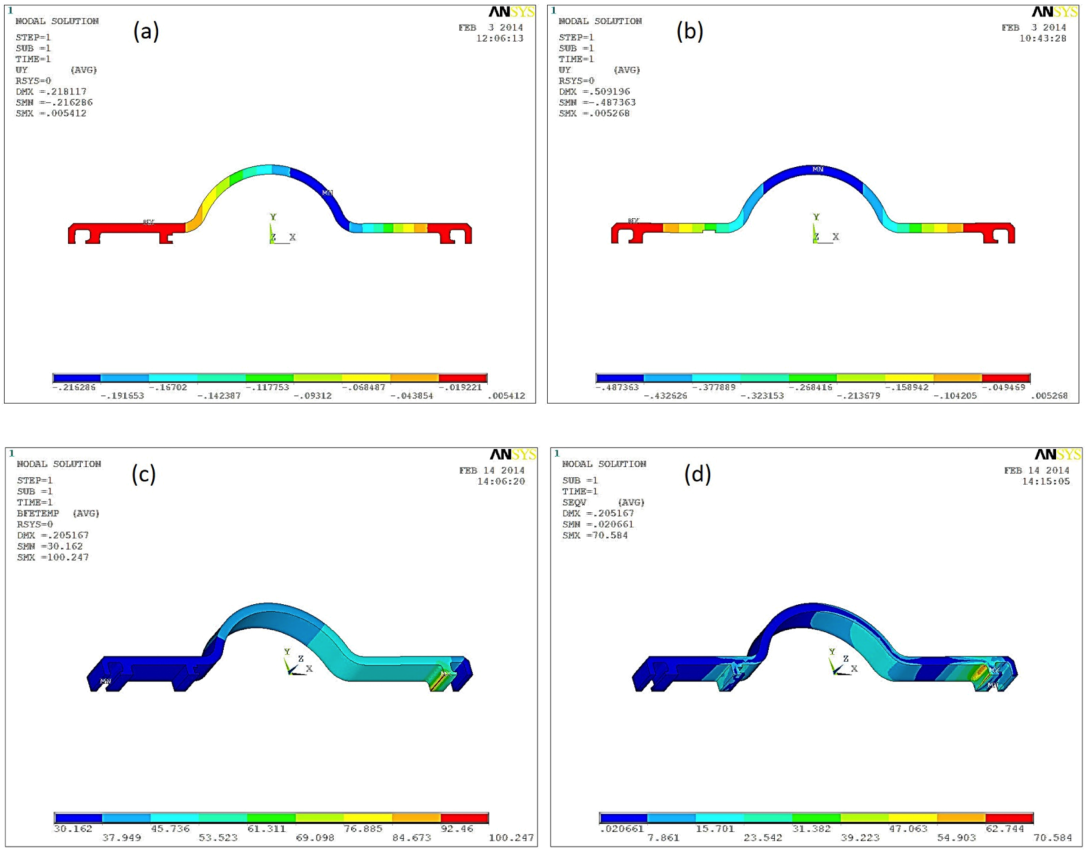

Figure 8.5: Estimation of vertical deformation for a typical beam pipe for LER (a) with and (b) without pump screen due to the atmospheric pressure of 0.1 MPa. Estimation of (c) temperature and (d) Von Mises stress while SR of 7.5 W mm^{-2} is irradiated with a height of 0.55 mm at the side wall of antchamer. The calculation is three dimensional. The heat convection to atmosphere is assumed to be about 5×10^{-6} W mm^{-2}K^{-1}, which is a typical one for a natural air flow. The temperature of atmosphere and cooling water are set to 25 °C. The convection coefficient to the cooling water is 0.01 W mm^{-2} K^{-1}. The flow rate of about 10 L min^{-1} is considered. The Young modulus, the Poisson ratio, the thermal conductivity and the thermal expansion rate of aluminum alloy are 7.2×10^{4} N mm^{-2}, 0.3, 0.21 W mm^{-1}K^{-1} and 23.4×10^{-6} K^{-1}, respectively.

manufacturing error of beam pipes after welding or brazing should be less than 2 mm in the horizontal plane and 1 mm in the vertical plane. The height of step at the joint should be less than 0.5 mm in the vacuum side (inside the beam pipe). The misalignment of the central axis between the beam pipe and the flange should be less than 0.5 mm. The tilt along the beam axis should be less than 10 mrad between the end flanges. The squareness tolerance at the end flange is less than 0.2 degrees.

8.2.7 Surface cleaning

Because getters are used as the main pump, as will be described in Sec.5, the reduction of gas desorption is important to avoid frequent conditioning of the getters and to prolong their life. A chemical polishing procedure, therefore, has been adopted to remove the initial oxide surface including a carbon compound. For copper beam pipes, after degreasing with Na_3PO_4 ($40 \sim 60$ °C) or a surfactant and washing with tap water, the surface was etched with a mixture of H_2SO_4 and H_2O_2 (room temperature). The etched depth is $1 \sim 5$ μm. Then the pipe is washed with deionized water (electric conductivity of less than 1 μS). Finally, the beam pipe is dried with dry nitrogen. Sometimes the beam pipe is wiped with a surfactant again after the chemical etching followed by washing with tap water. For aluminum-alloy beam pipes, on the other hand, after degreasing with alcohol or a surfactant, the inner surface was etched with NaOH and brightened with HNO_3 in order to remove damaged layer during the extrusion. Then the pipe is washed with tap water followed by deionized water, and dried with dry nitrogen finally. Otherwise, after degreasing with alcohol, the inner surface was etched with H_3PO_4-based solvent following the cleaning with a tap water. The chemical clearing described above is applied to every part after machining, such as flanges, SR masks, screens, which are faced to vacuum. All cleaning procedure is done before the welding and the assembling. Any contamination should be avoided after the assembling. The work should be done with a clean globe. In case of any contamination, the surface is wiped out with fiber-free cloth dipped with alcohol.

8.2.8 Type and typical layout

Beam pipes can be roughly divided into three types, that is, those for quadrupole and sextupole magnets (Type-Q), for bending magnets (Type-B) and for straight (drift) spaces (Type-S). Schematic structures of each type are shown in Fig. 8.6 (a)-(c). These beam pipes are connected through a bellows chamber in principle. In general, for a new beam pipe with antechambers, ports of ICF-70 UHV flanges with a feed-through are required to supply a current to a sheath heater in order to activate (heat up) NEG

strips inside of the pump channels. Ports of ICF-203 UHV flanges for ion pumps or rough pumps are also prepared at the bottom side of an antechamber. For a single-pipe beam pipe, on the other hand, ports of ICF-203 UHV flanges for ion pumps, cartridge-type NEG pumps and rough pumps are located at the bottom of the beam pipe. SR masks are prepared at the most downstream side of the beam pipe to make a shadow of SR to protect the flanges and bellows chambers downstream. Cooling water channels are at the both sides of the beam pipe. The Type-Q is a beam pipe for quadrupole magnets, sextupole magnets and correction (steering) magnets. The beam pipe is straight and has electrodes for the beam position monitor (BPM). The BPM calculates the beam orbit from the induced fields at four pickup electrodes, which are attached to a block with the same cross-section as the beam pipe. The newly-developed BPM block for the beam pipe with antechambers is presented in Fig. 8.7. The inset shows a pickup electrode. The copper BPM block is reinforced by two stainless-steel ribs. Alternatively, the aluminum BPM block together with ribs is machined from a single block. The pickup electrodes are attached to the block by a UHV flange (ICF-034) with a helicoflex-delta seal (Valqua Garlock Japan). The final calibration of the BPM will be performed using a circulating beam (i.e., the beam-based alignment). The BPM blocks are rigidly fixed to the quadrupole magnet. The beam pipe can expand longitudinally with a BPM block as a fixed point. The Type-B is the beam pipe for bending magnets. Each beam pipe has a curvature corresponding to that of the bending magnet. The typical Type-B beam pipe for LER has a curvature radius of 74.68 m and a length of 4.7 m. As described later, the Type-B beam pipes for LER has a grooved surface at top and bottom of the inner surface of the beam channel (see Sec. 7). The Type-B beam pipe for HER, on the other hand, has a curvature radius of 105.98 m and a length of 6.4 m. The Type-S is straight and is the beam pipe for the drift region, that is, the space between magnets. The Type-S beam pipe is simple, but the variety of lengths are required. Basically the sputter-ion pumps and vacuum gauges are attached to the Type-S beam pipes. The beam pipes in wiggler magnets can be classified to the Type-S. The SR hit at both sides of beam pipes. Ports for pumps are located at the bottom of antechambers. The straight beam pipe in the LER wiggler magnet has a clearing electrode at the top of the beam channel as also described in Sec. 7. Examples of a typical layout of beam pipes at an arc section (a part of lattice cell) for LER is shown in Fig. 8.8. This figure includes a Type-Q, a Type-B and a Type-S. Each chamber will be connected by end flanges together with a bellows chambers between them. There are two bellows chambers between a pair of quadrupole magnets. Considering an easy installation and alignment of beam pipes, the two bellows configuration is much preferable. The BPM block of the Type-Q is

rigidly fixed to the quadrupole magnet as described above. The Type-B, on the other hand, is only inserted into the magnet. For every types, the end flanges are fixed with supports to the floor. These supports are used to fix bellows chambers at the same time. The supports allows the beam pipes and bellows chambers to move freely along the beam axis. Some Type-S beam pipes have ion pumps, and each ion pump has a special support. The support for ion pumps has a spring action and can move more freely even on the horizontal plane.

8.2.9 Special beam pipe

Other than the major beam pipes described above, some special beam pipes are required in the rings. In the beam injection section, beam pipes to connect the chamber with a septum magnet inside (septum chamber) are prepared [45]. In the Super KEKB, the septum magnet is in vacuum, and no separation window is installed between the beam pipe in the ring and the septum chamber. A special beam pipes to merge the injection and the circulating beams with a slight angle is also required. Furthermore, a beam pipe with small electrodes (strip-line type) are newly developed for measuring the position of the injection beam (Fig. 8.9 (a)). The information of the beam position is expected to be help a stable beam injection cooperated with a feedback system. Beam pipes to abort the circulating beam has a titanium window with a thickness of 1 mm (Fig. 8.9 (b)) [46]. The ejected beams are damped in a beam damp which is shielded by iron blocks. In order to kick the beam for the beam injection or beam abort, a ceramics chamber with a thin titanium coating inside is manufactured. The horizontal beam size is measured using SR emitted from a bending magnet. A beam chamber with a mirror to extract the SR to the detector is installed at a straight section in each ring [47]. The diamond mirror with a water cooling paths is set in an antechamber at outside of the ring, and the impedance, therefore, is small (Fig. 8.9 (c)). A mechanism to adjust the mirror position is attached to the chamber. Since the vertical beam size is very small in the SuperKEKB, an X-ray line to measure the vertical beam size is also prepared [48]. The length of beam line is approximately 40 m. A special beam chamber to extract the X-ray is installed in the ring, which has a photon stop at the crotch. A sophisticated photon stop is designed to decrease the power density on the photon stop (Fig. 8.9 (d)). In order to suppress the background noises to the particle detector, several beam collimators are installed in each ring. The detailed will be discussed later in Sec. 9.

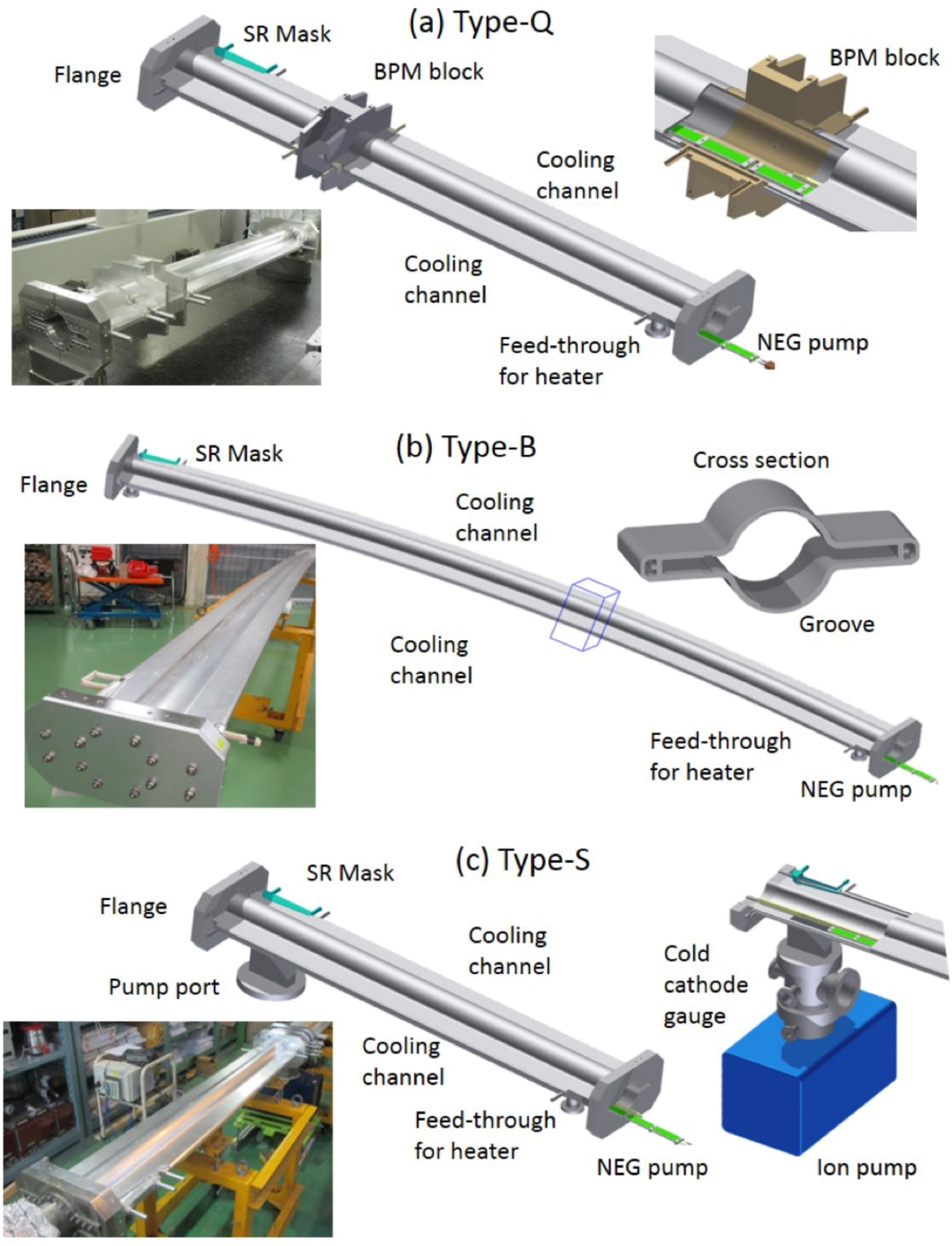

Figure 8.6: Schematic drawings of (a) Type-Q (b) Type-B and (c) Type-S beam pipe.

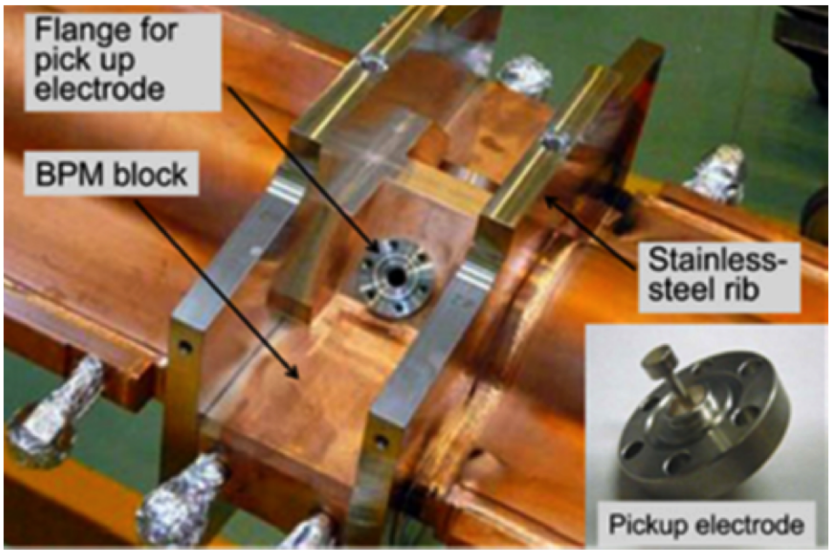

Figure 8.7: BPM block for a beam pipe with antechamber (copper).

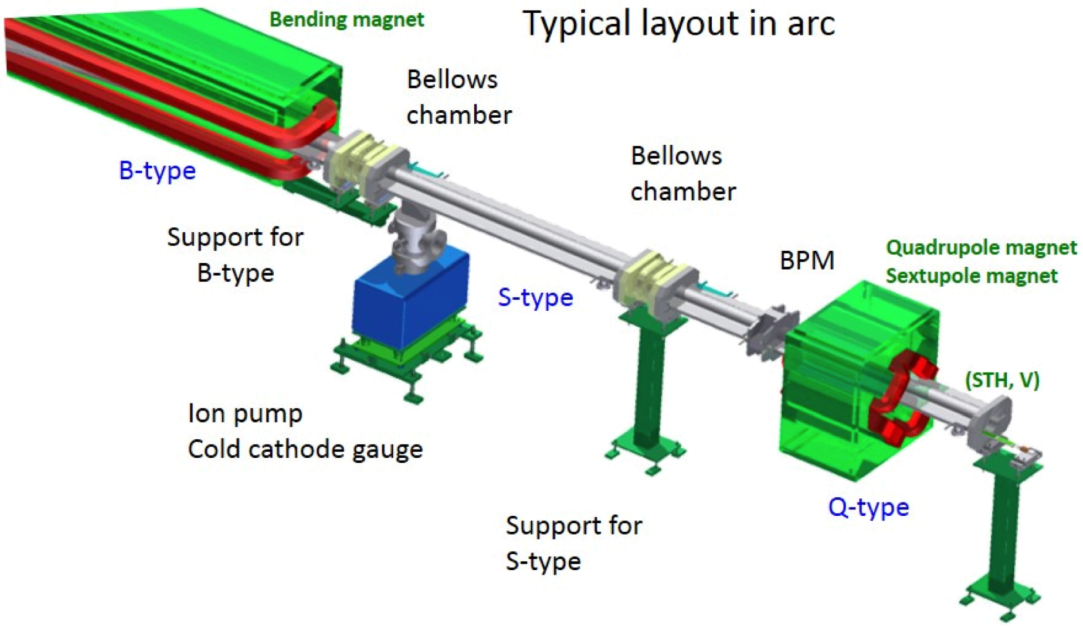

Figure 8.8: Typical layout in an arc section.

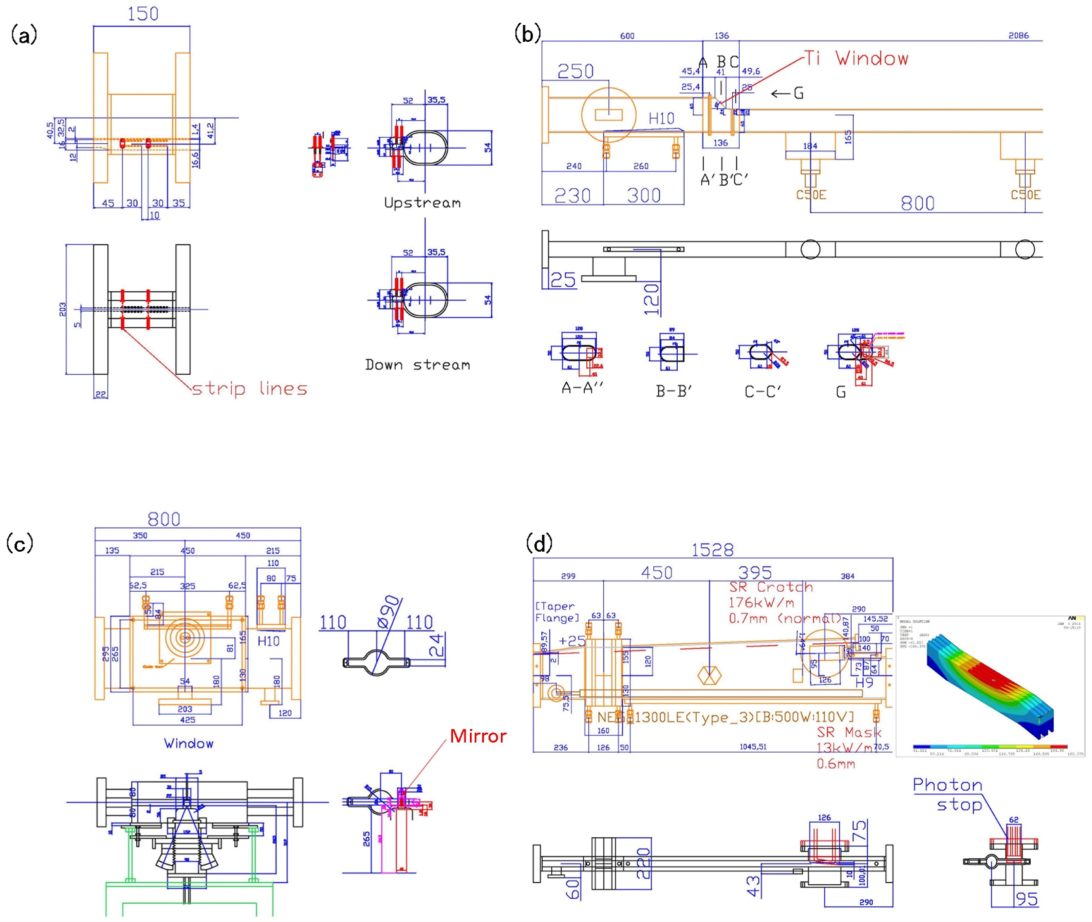

Figure 8.9: Design drawings of beam pipes for (a) beam injection, (b) beam abort, (c) SR beam size monitor and (d) branch chamber for X-ray beam size monitor.

8.3 Connection flange

Since the SuperKEKB operates with a short bunch length and a high bunch current, even gaps or steps at the connection flanges of beam pipes can be a measureable impedance source because the number of flanges are large, although the individual contributions may be small [42]. The Matsumoto-Ohtsuka-type (MO-type) flange can seal a vacuum at the inner surface to maintain a smooth current flow across a metal gasket [43][44][45], and provide much smoother connection than flanges with conventional fingers or metal O-rings [46][47]. The step inside expected structurally is 0.5 mm at most. Another advantage of this flange is that it can be applied to various cross sections other than a rectangle or a circle. A copper-chrome alloy (CrCu, C18200) and an aluminum-alloy (A2219-T851) flange have been developed instead of stainless steel for the SuperKEKB. This simplifies the manufacturing process of the beam pipes and also reduces Joule loss associated with the heating flanges, which was observed in beam tests in KEKB. The flanges are available to most of cross sections described in Sec. 1. A vacuum seal is achieved with a fastening torque less than $17 \sim 20$ Nm per bolt, similar to the case of a standard circular flange with the same diameter. The gaskets are made of annealed OFHC or annealed aluminum alloy (A5052-H34) with a hardness of $\mathrm{Hv} = 40 \sim 60$. An aluminum-ally and a copper-alloy flange for beam pipes for LER are shown in Fig. 8.10 (a) and (b). The gasket is fixed to the flange by two pins, and is make the connection work easy. Note that it was found in the experiment in a laboratory that the connection of copper-ally and aluminum alloy flange is not available. The vacuum seal was achieved in a room temperature, but after a baking at 150 °C for 24 hours, air leak was detected. The change of materials for gasket (pure copper, aluminum alloy) and fastening bolts (stainless steel, aluminum alloy, tin) had no effect. The connection of the flange with the same material is essential. For the beam pipes of HER, most of beam pipe are reused as it is, and a helicoflex-delta type gaskets are used for flanges. The MO-type flange are used for new antechamber-type beam pipes as shown in Fig. 8.1 (b) and (c).

8.4 Bellows chamber and gate valve

Bellows chambers are installed between adjacent beam pipes to ease beam pipe installation and to absorb any thermal deformation [48][49][50][51][52]. More than 1000 bellows chambers are used in one ring, and special attention is paid to the reliability of their RF shield. Because the beam current is large and the bunch length is small in the SuperKEKB, the heating of bellows chambers due to the higher-order mode

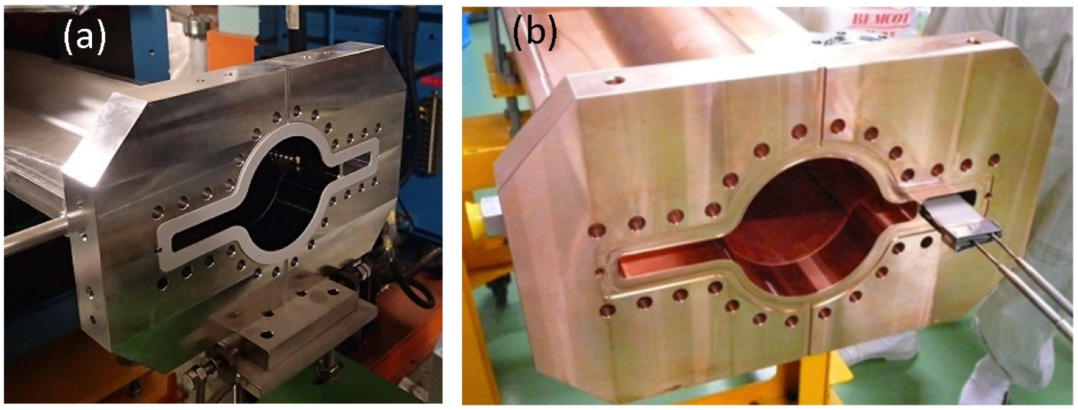

Figure 8.10: MO-type flanges for beam pipe with antechambers of (a) LER arc (aluminum alloy) and (b) wiggler section (chrome-copper alloy).

(HOM), especially TE-mode-like HOM, will become a serious problem. Heating of bellows caused by HOM had been actually observed already at the KEKB [9]. The new bellows chambers has a comb-type RF-shield structure that has a higher thermal strength than previously reported RF-shields [50][51][52]. The RF shield consists of thin, interlocking comb-teeth. A typical thickness of a tooth is 1 mm, and the gap between adjacent teeth is 2 mm. The radial thickness of the tooth is 8 mm, and the length is 14 mm. The overwrap of the comb-teeth is 6 mm at the nominal position. At the back side of teeth, another RF-shield fingers (Back fingers) are prepared to flow the DC or low-frequency current. The comb-type RF-shields can be used in various cross-sections of the beam pipe, such as a beam pipe with antechambers. A bellows chambers and the comb-type RF shield (inside view) are shown in Fig. 8.11 (a) and (b), respectively. The material of the RF-shield will be pure copper or aluminum alloy. The bellows is made of stainless steel (SUS316L) with a thickness of 0.1 mm. Gate valves will be indispensable to build a safe vacuum system. A gate valve also should have an RF-shield structure inside as bellows chambers. The VAT Series-47 type (VAT CO. Ltd.) have been used in KEKB and almost working well [9][10]. However, since the RF shield of existing gate valves are a finger-type, it may be difficult to fit an antechamber structure. Another problem is a heating of gate valves, which has been also sometimes observed in KEKB. Then the comb-type RF-shield is used as in the case of bellows chambers. Approximately 40 gate valves are installed in each ring. The gate valves are actuated by a compressed air. The beam stoppers for the safety system have a similar structure to the gat valves The bellows chambers and gate valves use MO-type flanges with the same cross section of beam pipes to be connected. No taper structure, there-

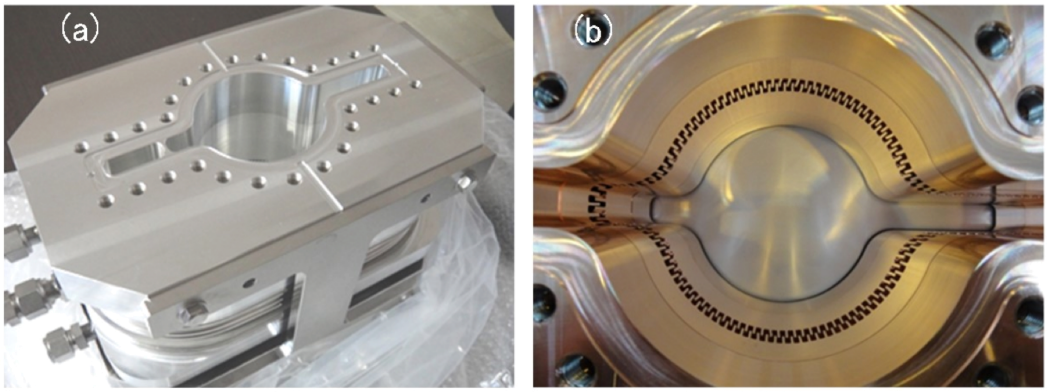

Figure 8.11: (a) Whole view and (b) inside view of a bellows chambers with a comb-type RF shield adapted to a beam pipe with antechambers.

fore, is required at both sides of them, and it contributes to decrease impedance. The material of flanges for bellows chambers are copper-chrome alloy or aluminum alloy, which are used for copper and aluminum-alloy beam pipes, respectively. Various types of bellows chambers and gate valves with comb-type RF-shields had been installed into the LER and HER of the KEKB and tested with beams [51][52]. The bellows chambers and gate valves did not cause problems, such as bursts of vacuum pressure due to arcing. Some bellows chambers with conventional finger-type RF shields were replaced by those with the comb-type, and a reduction in bellows temperature was observed.

8.5 Pumping Scheme

8.5.1 Pressure Requirement

Assuming that a beam pipe has a sufficient physical aperture, the beam lifetime due to the residual gases in the beam pipe is mainly limited by the bremsstrahlung process. The lifetime determined by this process must be much longer than a luminosity lifetime and a Touschek lifetime, and adequately long to meet an injection scheme. In this case, the life time, τ [s], is given by [53][54]

$$\frac{1}{\tau} = \sum_i \frac{1}{\tau_i}, \qquad \frac{1}{\tau_i} = c\frac{P_i}{k_B T}\sigma_B\left(Z_i\right)$$
$$\sigma_B\left(Z_i\right) = 4\alpha r_0^2 Z_i\left(Z_i+1\right)\left(\frac{4}{3}\ln\frac{\gamma}{\gamma_c} - \frac{5}{6}\right)\ln\left(183 Z_i^{-\frac{1}{3}}\right), \tag{8.1}$$

where τ_i is the lifetime due to an atom with an atomic number Z_i and a partial pressure of P_i.$\sigma_B(Z_i)$ is the cross-section of beam loss due to the bremsstrahlung process.

α, r_0, γ, γ_c are the fine structure constant (= 1/137), the classical electron radius (= 2.82×10^{-15} m), Lorentz factor and the limit of energy loss (=$\gamma\Delta$E/E), respectively, where ΔE/E is the RF bucket height. As indicated in Eq. (1), the larger the atomic number is, the larger the cross section is. The residual gases in a beam pipe during a beam operation comes from the photon stimulated gad desorption (PSD) process [33][55][56][57][58][59][60][61]. The main and important gas is, therefore, carbon monoxide (CO). For ΔE/E = 0.01 and T = 293 K, the following relation is obtained;

$$P\tau = 5.6 \times 10^{-6} \text{ [Pa Hours]}. \tag{8.2}$$

For example, to achieve a beam life time of 10 hours, an average pressure of about 5×10^{-7} Pa is required. The second important issue will be a background noise to a particle detector. The source of the back ground is a gamma ray or neutrons generated the spent particles, which are scattered by the residual gases. Heavy molecules, such as CO, are again major concern. Although any clear estimation has not been presented yet, a pressure less than 1×10^{-7} Pa will be required around the interaction region as KEKB [5][7]. From experiences, a pressure at just upstream side of a particle detector is more important than that at arc sections. In arc sections, a beam collimator system will be able to control the background noise to an extent. A pressure of on the order of 10^{-7} will be necessary in arc sections all the same. The next concern is ion trapping phenomena (instabilities) in the electron ring, HER [62]. From experiences in KEKB, the ion trapping phenomena sometimes occurred when some local region in a ring has a pressure on the order of 10^{-6} Pa. The phenomena strongly depended on a bunch fill pattern. The instability will be also suppressed by a bunch by bunch feed back system to some extent. It is, therefore, difficult to specify clearly the pressure to avoid the ion trapping phenomena. Here necessary pressures are assumed to be on the order of 10^{-7} Pa in average and 10^{-6} Pa locally based on the experience. From considerations above, a goal average pressure with design beam currents is set at about 5×10^{-7} Pa for CO for both rings at arc sections. For this average pressure, it was also found that a fast ion instability in HER would be suppressed by a bunch-bunch feedback system.

8.5.2 Pumps

The main process of gas desorption during the beam operation is photo-desorption, i.e., desorption caused by SR [33][55][56][57][58][59][60][61]. The SR photon line densities (flux) along the ring for one lattice cell are presented in Fig. 8.3 (a) and (b) for LER and HER, respectively. The average photon flux in arc sections is approximately 6×10^{18} photons $\text{s}^{-1}\text{m}^{-1}$ for both rings (see Table 8.1). If we assume a photo-desorption coefficient (η) of 1×10^{-6} molecules photon^{-1}, the linear gas desorption is approximately

2×10^{-8} Pa $m^3s^{-1}m^{-1}$. In order to achieve the required pressures described above, therefore, a linear pumping speed of approximately 0.1 $m^3s^{-1}m^{-1}$ is required for CO. Note that, in the KEKB, η was found to have decreased with the beam dose down to less than 1×10^{-6} molecules photon^{-1} [9]. In order to effectively evacuate the long, narrow beam pipes, which have a limited conductance, a distributed pumping scheme using a strip-type non-evaporable getter (NEG) ST707 (SAES GETTERS Co. Ltd.) is adopted as the main pump in the LER [63]. A strip-type NEG can be used irrespective of the presence of magnetic fields [64][65], unlike a distributed-type ion pump. Cartridge-type lumped NEGs are also used for the straight section, such as a wiggler section, as necessary. Note that NEG-coated beam pipes, which create pumping action to the inner surface, have been recently used in several accelerators [66][67][68]. However, the small absorbing capacity of the coating can be a problem for relatively high gas-loaded machines [68]. The pumping system for the HER is the same as that used in the KEKB. The main pump is also a NEG-type pump, but the pumping scheme is a combination of strip types for Type-B beam pipes and lumped cartridge-type NEGs for Type-S and Type-Q ones [5][6]. For beam pipes at arc sections, the SR hits only the outside of the ring. Therefore, in the case of beam pipes with antechambers, the antechamber located at the inside of the ring can be effectively used as a pump channel (see Fig. 8.1). A screen with many holes of 4 mm diameter that shields the pump from the beam is installed in the antechamber between the pump and the beam. The thickness of the screen is 5 mm, and the conductance is approximately 0.2 m^3s^{-1} per 1 m. The thinner screen has larger conductance, but the leakage of HOM is larger at the same time. Generally, the thickness of holes should be larger than the diameter to work as an RF shield. The screen is inserted from the end flange, and tightly fit to the grooves formed in the antechamber (see Fig. 8.1). For regions where the cross sections of beam pipe frequently change and the HOM is likely to be excited, the screen touches the beam pipe through RF-shield fingers in the grooves. The schematic drawings of pump channel is presented in Fig. 8.12. In order fit to the various lengths of beam pipes, the screen consists of some modules with a typical length of 1 m. For straight sections, where the SR hits both side walls of the beam pipe, on the other hand, the pump ports are placed on the bottom of the antechambers. The pump port also has a screen for RF shielding at the entrance of the port. The screen has lots of holes with a diameter of 5 mm. For the pump channel with a full height of 14 mm, a pump assembly using multi-layered NEG strips was designed as shown in Fig. 8.13 [69]. Indirect heating with sheath heaters was considered instead of direct Joule heating in order to safely activate the NEG strips in the narrow space. A pump assembly consisted of several modules of NEG strips, each approximately 300 mm in length, which easily followed

the curvature of the Type-B beam pipe and the change in length caused by thermal expansion during the NEG activation. The total length of the assemblies to be fitted within the beam pipes ranged from 0.6 m to 3 m. The effective area of the NEG surface in an assembly is approximately 0.1 m2 per 1 meter. The linear pumping speed of the assembly for nitrogen (N2) just after an activation was approximately 0.2 $m^3s^{-1}m^{-1}$ (i.e., 2.0 $m^3s^{-1}m^{-2}$ for the NEG surface). Therefore, according to the data in the ST707 Catalogue [63] the pumping speed for carbon monoxide (CO), which is a main gas component in the photo-desorption process, was expected to be approximately 2.0 $m^3s^{-1}m^{-1}$ (i. e., 20 $m^3s^{-1}m^{-2}$ for the NEG surface) just after an activation. The combined linear pumping speed expected with a screen is, therefore, approximately 0.1 and 0.18 $m^3s^{-1}m^{-1}$ for N2 and CO, respectively. If gaps between the NEG assemblies and the length of the bellows chambers are taken into account (approximately 20 % in the ring), the effective linear pumping speed along the beam pipe is approximately 0.08 and 0.14 $m^3s^{-1}m^{-1}$ for N2 and CO, respectively. The frequency of the NEG activation at a steady state is roughly estimated in Sec. 13. To evacuate non-active gases and to enable more efficient evacuation in relatively high pressure regimes, sputter ion pumps with a nominal pumping speed of 0.4 m^3s^{-1} (0.2 m^3s^{-1} at 10^{-8} Pa) are provided as an auxiliary pump and positioned approximately every 10 m along the ring. The combined linear pumping speed expected with a screen is approximately 0.13 $m^3s^{-1}m^{-1}$ for CO. Figure 8.14 (a) shows the effective pumping speed and the obtained pressure for one lattice cell of LER with the photon flux as shown in Fig. 8.3 (a), where a beam pipe with antechamber and the distributed pumping speed of 0.12 $m^3s^{-1}m^{-1}$ are assumed. The conductance of 1 m beam pipe is approximately 0.095 m^3s^{-1}. Owing to the distributed pumping system, almost the constant pumping speed of 0.11 $m^3s^{-1}m^{-1}$ is obtained. The average pressure is approximately 2.3×10^{-7} Pa. For HER arc sections, the pumps are basically reused as it is. The main pumps are lumped pump using NEG cartridge with a pumping speed of 0.2 m^3s^{-1}. The combined linear pumping speed expected with a screen is approximately 0.1 $m^3s^{-1}m^{-1}$ for CO. The distributed pumps using NEG strips are used only for Type-B beam pipes. Two strip lines are used along the pump channel. The combined linear pumping speed with a screen of 0.13 $m^3s^{-1}m^{-1}$ is expected. For HER, however, since quadrupole and sextupole magnets are long and only lumped pumps are used there. Figure 8.14 (b) shows the effective pumping speed and the obtained pressure for one lattice cell of HER with the photon flux as shown in Fig. 8.3 (b), where a beam pipe with a race-track shape is assumed. The conductance of 1 m beam pipe is approximately 0.055 m^3s^{-1} and smaller than the case of LER. Since the lumped pumping scheme is used, the fluctuation of pressure is large. The average linear pumping speed is 0.075 $m^3s^{-1}m^{-1}$. The average

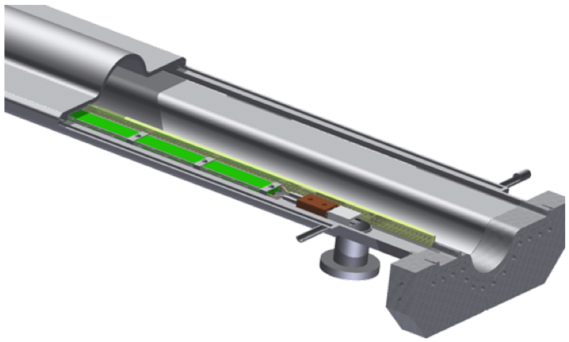

Figure 8.12: Schematic drawing of a NEG strip in an antechamber and a screen.

pressure is approximately 4.1×10^{-7} Pa. In some locations, the pressure is higher than 1×10^{-6} Pa. For comparison, if an antechamber-type beam pipe as shown in Fig. 8.1 (b) is used, and if the distributed pumps are adopted as in the case of LER described above, the effective pumping speed and the pressure as indicated in Fig. 8.14 (c) are obtained. The average linear pumping speed and the average pressure are 0.11 $m^3s^{-1}m^{-1}$ and 2.8×10^{-7} Pa, respectively. A more constant pumping speed is obtained compared to the case of Fig. 8.14 (b). The rough pumping system, which is used for the evacuation near atmospheric pressure regime, is completely oil-free and is based on a turbo-molecular pump (0.2 m^3s^{-1}) and a scroll-style dry pump (0.25 m^3 min^{-1}). A rough pumping port is located every 40 m along the ring. The rough pumping unit is portable, and the unit is detached from the ring after the starting up process, that is after the NEG activation. A rough pumping scheme will follow that of the KEKB [5][7].

8.6 Monitor and control system

8.6.1 System configuration

In general, antiquated devices are renewed as a priority while reusing the devices in TRISTAN or KEKB as much as possible. A Computer Automated Measurement And Control (CAMAC) system and VersaModule Eurocard (VME) computers had been used so far as a data logger and Input Output Controllers (IOC) of Experimental Physics and Industrial Control System (EPICS) [70], respectively. They will be replaced with CompactRIO (cRIO) [71] and F3RP61 [72], which is a Linux CPU module of Programmable Logic Controller (PLC), respectively. Figure 8.15 shows the configuration of the vacuum control system. The control system of one ring is divided into 12

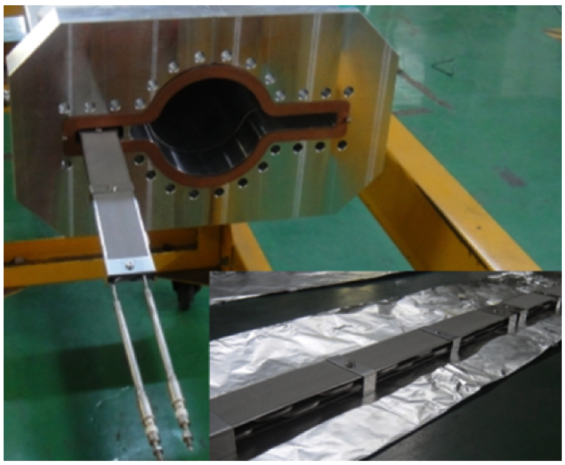

Figure 8.13: Newly developed three-layer NEG strip for antechamber with a height of 14 mm.

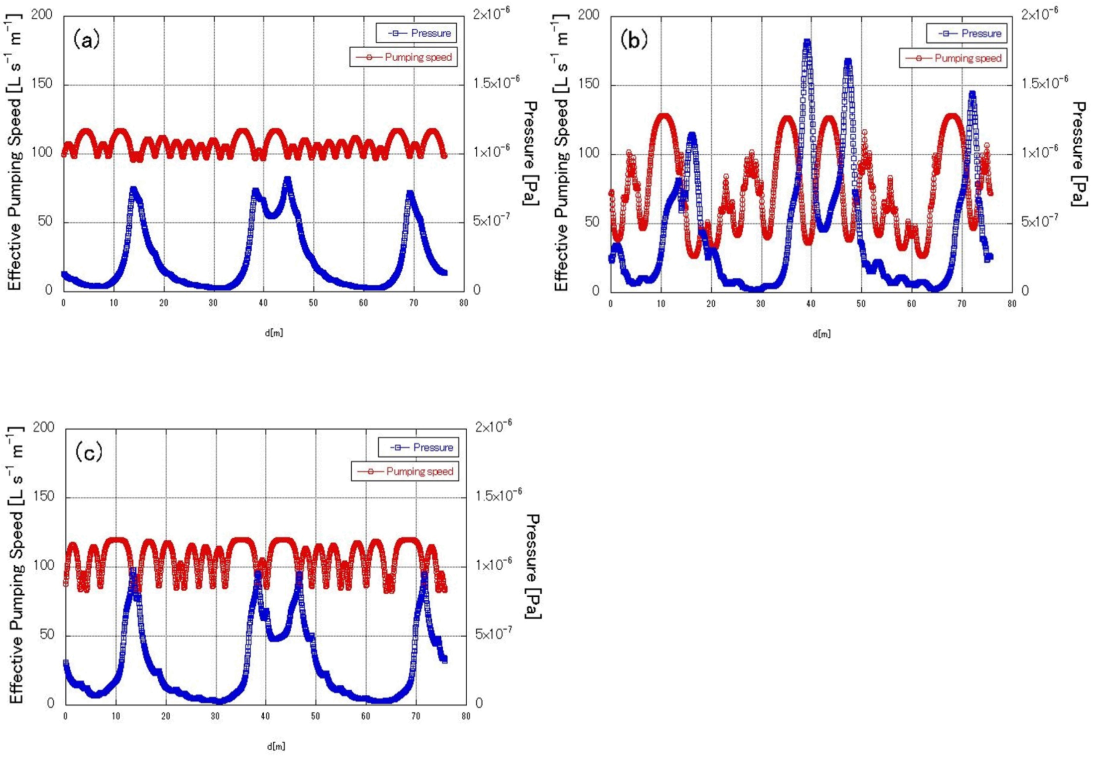

Figure 8.14: Effective pumping speeds and expected pressures in a lattice cell of (a) LER and (b) HER, where the photon flux as shown in Fig 8.3 and the η of 1×10^{-6} molecules photon^{-1} are assumed, and (c) is the result when an antechamber structure is used for HER.

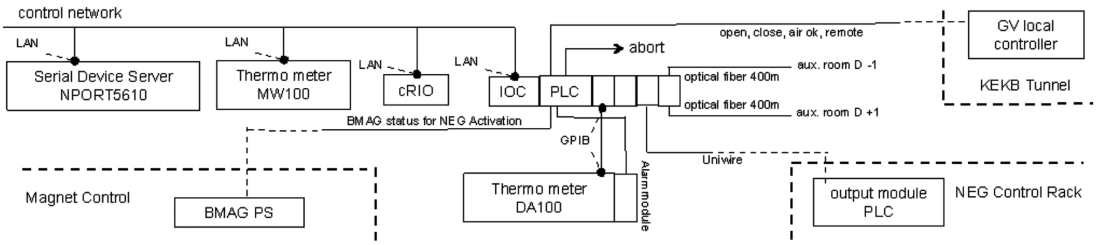

Figure 8.15: Configuration of control system of vacuum components.

branches, and each branch has two cRIO units. One cRIO unit is used for data acquisition of pressures of vacuum gauges, discharge currents and high voltage (HV) statuses of ion pumps, and flow rates of flow meters. Another cRIO unit is used as a controller of power supplies for NEG activation. The cRIO system is light and compact, and the channel density is high compared with the CAMAC. A PLC unit is used for the HV and interlock controls of vacuum gauges and ion pumps, the open/close and interlock controls of gate valves, the interlock controls of power supplies for NEG activation, and so on. Control System Studio (CSS), which is an Eclipse-based collections of tools to operate large scale control systems, is used for the graphical user interface (GUI) of the control panel on a terminal. The static displays based on Motif Editor and Display Manager (MEDM) that has been basically used in KEKB is replaced by CSS. The operator can control the components, and check the status of them from any terminal connected to the network. Control cables of components are laid from the branch on the ground into the tunnel. They are non-halogen and flame retardant, and also has a high resistance to radiation.

8.6.2 Monitoring system

The monitoring items and numbers in the main ring are summarized in Table 8.3. Approximately 300 Cold Cathode Gauges (CCG, C−5 or CG−28, DIAVAC) are located approximately every 10 m in each ring to monitor the total vacuum pressure. Most of CCG will be reused as it is. The measurable pressure range is from 10^{-2} to 10^{-8} Pa. All of these monitors will measure and record pressures every 1 or 2 seconds. A high speed measurement system is also built using Field-Programmable Gate Array (FPGA) resource on cRIO. This system can acquire the all pressure data with 100 Hz. That enable us to identify a CCG which detect a pressure rising first, or to narrow down the point of an air leakage. The pressure data for 20 minutes are stored in a circular buffer on a memory of each cRIO.

Monitor and control item	LER (positron)	HER (electron)
Vacuum switch (VSW)	31	33
Gate valve (GV)	33	35
Beam stopper	2	2
Ion pump (IP)	307	307
Cold cathode gauge (CCG)	307	307
Power supply for NEG activation	17	24
Temperature sensor	1884	1444
Flow meter (existing)	376	
Flow meter (new for wiggler section)	383	

Table 8.3: Control and monitoring items in vacuum system.

Other than CCG for measuring total pressures, one or two residual gas analyzers (RGA) are also installed in the ring to identify the component of desorbed gas. The controller is located in the tunnel and communicate with an Ethernet interface. In order to measure the accurate total pressure and also to compare with the reading of CCG, some extractor gauges (IONIVAC IM540, Oerlikon Leybold Vacuum) are prepared at arc section.

Sputter ion pumps (PST−400, ULVAC Japan) are also installed approximately every 10 m at the same point of CCG in the ring. The discharge current of ion pumps can be used as a measure of pressures in the range from 10^{-4} to 10^{-6} Pa. The ion pump runs normally at a pressure lower than 10^{-4} Pa, but a high voltage (+5 kV) can be applied temporally from 10^{-3} Pa. Most of ion pump controllers and power supplies are reused [73]. These controllers will be replaced with new ones gradually. The new controller make the pressure measurement possible even in the range of 10^{-8} Pa.

The main pump is the NEG strips and cartridges distributed along the ring as described above. The power supply for the activation of NEG will be reused as it is. However, since a variety of heaters are used for the activation this time, many types of transformers are newly installed into the tunnel in order to fit the voltage with each heater. The currents of heaters are controlled by the pattern generator embedded in the power supply. Since AC voltage is usually used for the NEG activation, the NEG or the heaters in active magnets oscillate by the magnetic field, and are sometimes damaged. In LER, rectifiers will be installed between the transformer and NEG heater in the bending and quadruple magnets. The rectifiers cannot be used so easy in HER due to the difference of activation mechanism. NEG pumps within ±50 m from the collision point will be activated by DC power supplies so as not to make noise to the

quench monitors of superconducting focusing magnets.

Temperatures at approximately 3300 points in various vacuum components are monitored by a platinum resistance thermometer detector (RTD, Pt 100, Class B). As for the temperature monitoring, a data logger system (DA100, YOKOGAWA) is reused as it is. An asynchronous device support is newly developed to control them with a GPIB module of the PLC unit. The temperature data measured with DA100 is used for a trigger of the beam abort in combination with the flow rate of cooling water (see below).

The flow rate of cooling water is monitored using a wheel-type flow meter. The frequency of rotation of the wheel is proportional to the water flow linearly, and is converted to the DC voltage of 0 -10 V. The flow rates are monitored at approximately 370 points near the inlet valves all along the tunnel. The typical flow rates are 20 L min^{-1}. In the wiggler section, however, the flow rate should be increased up to approximately 120 L min^{-1} to absorb the high SR power. A header system, therefore, is prepared for the wiggler sections. One header has 6 - 10 branches of cooling path. The flow rate is measured at each branch, and the measurements points are approximately 380 in the wiggler sections.

Gate valves divide the ring into 33 $-$ 35 sectors to ensure serviceability of the vacuum components in each sector. Two beam stoppers are prepared in each ring as a safety system. The gate valves and the beam stoppers are driven by a compressed air with a pressure of 0.6 MPa. The open or close status and the air pressure is monitored using a PLC unit. At least one vacuum switch is installed in the sector between two gate valves to check the vacuum status of the sector.

The beam collimators require more delicate monitoring and control. The position of jaws should be adjusted watching the back ground noise of particle detector and beam life time. Since there are over 10 collimators in each ring, they should tuned systematically. The requirement to the positional accuracy is also high. The final form of the control system of beam collimators are under consideration.

The electron cloud effect is an important issue in the positron ring, LER (see Sec. 7). The experimental studies using the LER should be useful for understanding the effect. Several electron monitors [74] will be installed in the LER arc sections or straight sections in the future.

8.6.3 Interlock system

A normally closed interlock logic with digital I/O modules and the sequence CPU module of the PLC unit is built.

Vacuum switches are used to check a vacuum state in a sector between two gate

valves. They detect pressures higher than 1000 Pa. The high voltage of CCG can be applied when the vacuum switch closes in the corresponding sector. The CCG controller returns normal discharge status when the pressure is less than approximately 10^{-3} Pa. The controller turns off the high voltage when the discharge does not move to the normal state within a certain time to avoid the pollution and damage.

When some CCG in the sector are normal, the high voltage can be applied to ion pumps in the same sector, and also the activation of NEG become available. If the pressure in the sector get worse by any reasons, the high voltage of the CCG goes down first. The high voltage of the ion pumps and the output of the power supply for the NEG activation also go down by the interlock logic. Since the power supplies for the NEG activation in HER are not DC as mentioned, the logic checks the status of the magnets at the same time. When the pressure get worse further and the high voltages of several CCG go down, the gate valves at the ends of the sector are closed. The sequence CPU checks the statuses of two adjacent sectors using FA Link. The gate valve can be opened only when the statuses in both sectors are normal.

A normal-close beam abort logic is established with a ladder sequence program. The sources of the trigger signal are temperature sensors, flow meters, gate valves and beam stoppers. For temperature, the data logger has two thresholds, that is, a lower and a higher level. The system triggers an alarm when the temperature exceed the lower level or it detects a break of the sensor. The system triggers an abort signal when the temperature exceed the higher level. The flow rates was one of triggers for the beam abort in KEKB. However, metallic powders sometimes clogged the waterwheel, and it had also sometimes triggered the beam abort signal. In order to avoid the unnecessary trigger, an interlock logic is built where the system determines whether the measured flow rate is true or not by a combination of the flow rate and temperature sensors correlated with the flow meter.

8.7 Mitigation of Electron cloud effect

he electron cloud effect (ECE) has been a critical issue in recent high-intensity positron/proton rings [15−17, 35]. The single-bunch instability caused by the electron cloud is naturally a serious problem for the SuperKEKB, and more thorough countermeasures than ever before are required [16, 17]. The multi-bunch instability can be also excited, but it is expected to be cured by a bunch by bunch feedback system.

The threshold of the electron density in the beam pipe that excites the instability, $\rho_{\rm th}$ [electrons $\rm m^{-3}$], is given by the following formula [75] :

$$\rho_{th} = \frac{2\gamma\nu_s\varpi_{ey}\sigma_z/c}{\sqrt{3}KQr_e\langle\beta\rangle L}, \omega_{\rm ey} \equiv \sqrt{\frac{\lambda r_e c^2}{\sigma_y(\sigma_x+\sigma_y)}} \tag{8.3}$$

where $\gamma = 7828$, $\nu_{\rm s} = 0.0244$, $\omega_{\rm ey} = 5.5{\times}10^{11}$ Hz, $\sigma_{\rm z} = 6$ mm, $c = 3{\times}10^8$ ms^{-1}, K ˜ 11, Q ˜ 7, $\mathrm{r_e} = 2.8{\times}10^{-15}$ m $L = 3016$ m, $\lambda = Q_{\rm b}/2/\sigma_{\rm z} = 5.2{\times}10^{12}$ C m^{-1} and $Q_{\rm b} = 1.4{\times}10^{-8}$ C. The $<\beta>$ is the average beta function in the ring. For $<\beta> = 10$ m, $\rho_{\rm th}$ is $3.7{\times}10^{11}$ electrons m^{-3}. However, both the electron density in the beam pipe, ρ, and β changes along the ring. That means that the more exact criterion of the instability should be evaluated from the tracking simulation considering the distribution of ρ and βalong the ring as described later. In the design of vacuum system, the target of the electron density is set to $1{\times}10^{11}$ electrons m^{-3} as the first approximation.

Various kinds of experiments related to the ECE had been performed in KEKB [22, 74, 76−79]. Based on the results, the expected electron density at arc and straight sections are estimated assuming a circular copper beam pipe, and they are summarized in Table 8.4 [80]. The expected average density is $6{\times}10^{12}$ electrons m^{-3}, which is much higher than the threshold. That means more rigorous countermeasures than before are required to reduce the electron density. Here described are the countermeasures adopted in the main ring.

8.7.1 Antechamber structure

The electron cloud is initially created by photoelectrons emitted from the surface being irradiated by SR. The antechamber structure, therefore, helps to minimize the effects of the photoelectrons because their emission points, which are on the side wall, are far from the beam orbit, and the attractive electric field induced by the beam is weak there. Furthermore, the surface of the side wall is roughened to a roughness (Ra) of between 7 μm and 20 μm to suppress photon scattering [81].

A copper beam pipe with an antechamber was installed into the KEKB positron ring, and the electron density was experimentally estimated using an electron monitor. A typical result is presented in **Fig. 8.16**, where the measured electron current corresponds to the electron density around the beam. The electron monitor is located at the bottom of the beam channel [74]. The result was obtained in an arc section where photon flux of $8{\times}10^{15}$ photons m^{-1} s^{-1} is irradiated. As shown in the figure, the electron density in a copper beam pipe with antechamber reduced by two orders of magnitude compared to the case of a circular copper beam pipe at the low current regions less than 100 mA.

In a high bunch current regime, however, secondary electrons due to electron impact play a major role in forming the electron cloud. The electron density increases by a

Sections	Length [m]	Occ. length [%]	n_e (circular) [e^- m^{-3}]	Countermeasures: Ante (1/5)	TiN (3/5)	Sol. (1/50)	Gr. (1/4)	Elec. (1/100)	n_e (expected) [e^- m^{-3}]	Pipe materials
Drift space (arc) Cu (straight)	1629	54	8×10^{12}	•	•	•			2×10^{10}	Al (arc)
Corrector mag. Cu (straight)	316	10	8×10^{12}	•	•	•			2×10^{10}	Al (arc)
Bending mag.	519	17	1×10^{12}	•	•	•			3×10^{10}	Al
Wiggler mag.	154	5	4×10^{12}	•	•		•		5×10^{9}	Cu
Quadrupole and Sextupole mag. Cu (straight)	254	9	4×10^{10}	•	•				5×10^{9}	Al (arc)
RF cav. section	124	4	1×10^{11}		•	•			1×10^{9}	Cu
IR	20	1	5×10^{11}		•	•			6×10^{9}	Cu, Al
Total[a)]	3016	100								
Average[a)]			6×10^{12}						2×10^{10}	

a) Existing regions (reused regions) are neglected. The average density is approximately 3×10^{10} e^- m^{-3} if they are included.

Abbreviations;

RF cav. Section: Beam pipes around RF cavities, IR: Interaction region

Occ. length: Occupied length

n_e (circular): Electron density expected for circular beam pipe (copper)

n_e (expected): Electron density expected after applying countermeasures

Ante: Antechamber structure

TiN: TiN coating

Sol.: Solenoid winding

Gr.: Beam pipe with grooved surface

Elec: Beam pipe with clearing electrodes

Average: Averaged values weighted with the lengths of corresponding sections

Table 8.4: Countermeasures used to minimize ECE in LER. The circular dots indicate the applied countermeasures for each sections in the ring.

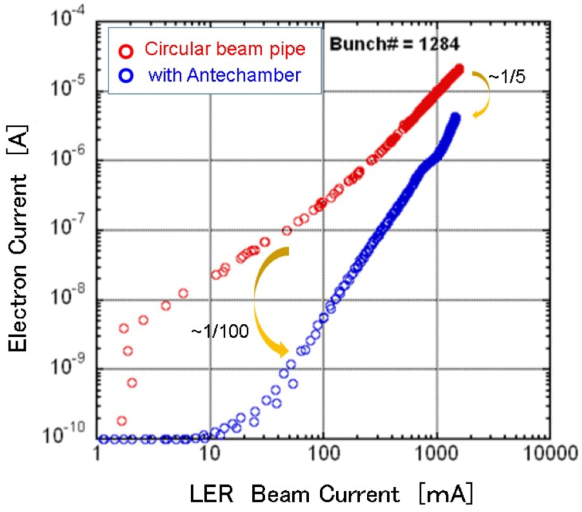

Figure 8.16: Typical results of measured electron currents for a circular copper beam pipe and a copper beam pipe with antechamber installed in an arc section as a function of beam current, where the number of bunches is 1284. The electron current reflects the electron density around the beam.

chain of electron emissions, that is, by multipactoring [76, 82, 83]. Actually, as also shown in Fig. 8.16, the electron density in the beam pipe with antechamber at a high beam current region (larger than 1000 mA) reduced to only approximately 1/5 compared to the case of a circular beam pipe.

8.7.2 Solenoidal magnetic field

A solenoidal magnetic field along beam pipes is very effective at preventing multipactoring, and was successfully worked at the KEKB and PEPII [35, 84, 85]. It was found that the electron density around a beam decreased by several orders of magnitude when a uniform axial magnetic field was applied to a circular copper beam pipe [74]. A typical result is presented in Fig. 8.17. The result was obtained in an arc section. Considering the gaps between the adjacent solenoids and the regions for the polarity change, the reduction efficiency in the electron density was actually expected to be approximately 1/50 for the solenoid. Since the present design of beam pipes with antechambers has no pumping port at a beam channel, more uniform magnetic field can be formed compared to the case of present KEKB.

The solenoid method, however, is available only in drift regions (field-free regions) of the ring, that is, for Type-S beam pipes, and partially for type-Q. Solenoid windings in magnets are not considered at present.

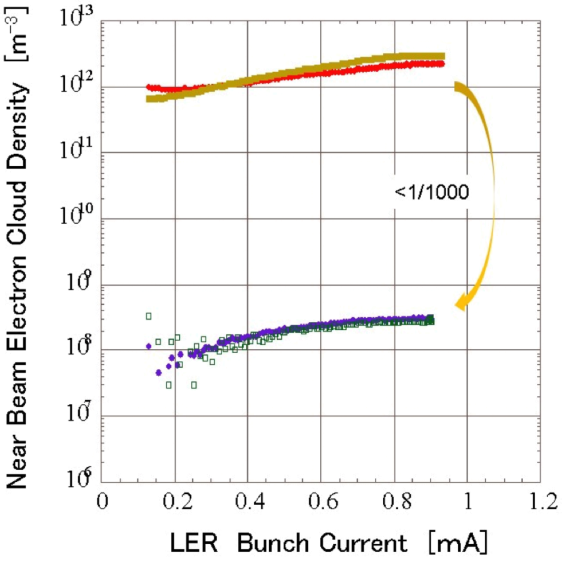

Figure 8.17: Typical results of measured electron densities around the beam with and without solenoid field of approximately 50 G as a function of bunch current.

8.7.3 TiN coating

Another way to suppress the secondary electron emission is to coat the inner surface with materials that have a low secondary electron yield (SEY), such as titanium nitride (TiN), NEG materials, or graphite (carbon) [35, 77, 86−96]. These coatings can be used not only in drift regions and also inside magnets. It should be noted that a bare aluminum alloy has a much higher SEY than copper, and any coatings are indispensable [35].

Various kinds of surfaces have been studied so far. One of the promising and interesting candidates is the coating of NEG materials (Ti-Zr-V, materials used for NEG), which has been mainly developed in CERN and is commercially available through SAES Getters. Co. Ltd. [35, 86, 87, 89, 90, 94, 95]. The coating of NEG materials (we call it NEG coating hereafter) has the maximum SEY ($\delta_{\max}$) of 2.0 at first, but decreased to about 1.1 just after an activation at 200°C for 2 hours [86]. The NEG coating will be applied to the beam pipe at the experimental region and at the worm section in the LHC [87]. Recently, carbon coating is intently studied in CERN for SPS proton ring [35, 91−94]. It is reported that the carbon coating has a low $\delta_{\max}$ around 1.0 even before the electron bombardment. The reduction of electrons in a beam pipe with carbon coating is actually observed in the SPS [92]. The reduction of electrons in positron rings, however, is similar to that of NEG or TiN coating in the experiment in CESR-TA [94]. TiN coating has been used commonly to decrease the SEY [35, 77, 88,

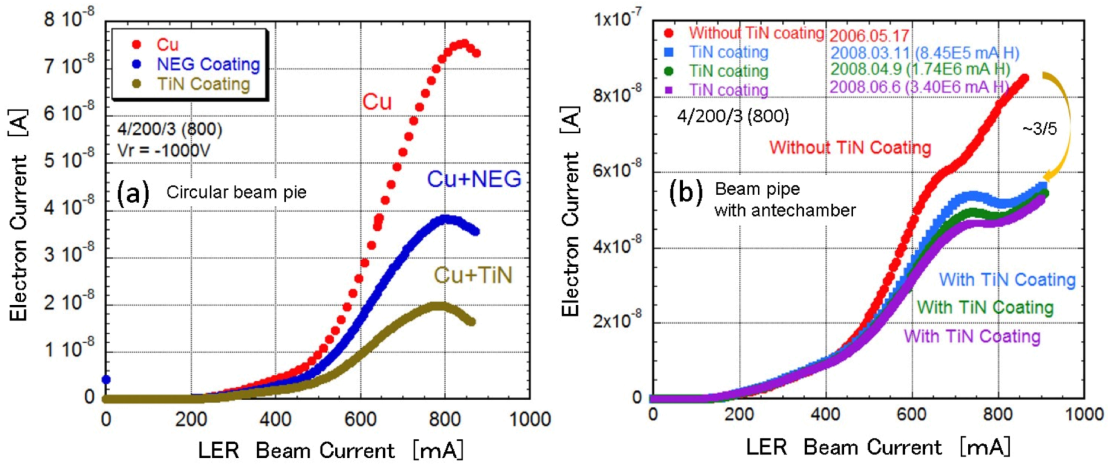

Figure 8.18: (a) Typical results of measured electron currents for a circular copper beam pipe without coating, with NEG coating and with TiN coating installed in a straight section as a function of beam current, where little SR is irradiated. (b) Results for a copper beam pipe with antechambers without and with TiN coating at different aging times installed in a wiggler section as a function of beam current. The electron current reflects the electron density around the beam. The number of bunches is 800 for both cases.

90, 94, 95, 96]. The TiN coating has been used in the LER beam pipes of PEP-II [88] and the coating technique is well developed. After a sufficient aging process, a SEY of approximately 1.0 is expected for the TiN coating [35, 96].

Circular copper beam pipes with NEG or TiN coatings were installed in the arc and straight section of the KEKB positron ring for tests, and the number of electrons around the beam was measured and compared [77, 89, 90]. A typical result in a straight region is shown in Fig. 8.18 (a), where the effect of SR is negligible. The electron numbers in the beam pipes with the TiN coating and the NEG coating were approximately 1/3 and 2/3, respectively, of that for a copper beam pipe without any coating. The TiN coating showed a similar result on an aluminum beam pipe. The TiN coating seemed to be the most promising coating at present.

The electron numbers around the beam were also measured for a copper beam pipe with antechambers with and without TiN coating where the SR 8×10^{14} photons m^{-1} s^{-1} was irradiated in the antechamber. TiN was coated only in the beam channel. The result is presented in Fig. 8.18 (b). TiN coating reduces the electron density by a factor of 3/5 at the high current region.

8.7.4 Grooved surface

It was reported recently that a grooved surface is very useful to suppress the electron cloud, especially in a dipole-type field, such as a bending magnet and a wiggler magnet [35, 78, 95, 97−99]. The grooved surface reduces the SEY geometrically. The SuperKEKB has long wiggler sections (˜150 m) and approximately 120 bending magnets (˜520 m). Considering the relatively high electron density in the dipole field, a reduction in the electron density in these regions is not negligible.

Triangular-type grooved surfaces with varying geometrical parameters (such as the angle of the triangles, the tip roundness and the pitch of the grooves) and surface conditions (i.e., with or without TiN coating) have been investigated in a wiggler magnet of the KEKB positron ring and also in the laboratory (magnetic field free) [78]. A result obtained in a wiggler magnet is presented in Fig. 8.19 (a). It was found a grooved surface with TiN coating can reduce the electron density by a factor of 2 compared to that for a plain copper surface. The sharper the tip and the smaller the tip roundness are, the more prominent the reduction is. The TiN coating on the grooves enhanced the reduction of electron density. A reduction in electron density by the use of grooved surfaces has also been experimentally demonstrated in CESR-TA, at Cornell University [94, 95, 99, 100]. In the SuperKEKB design, the grooved surface is adopted for beam pipes in the bending magnets in the arc sections.

A cut model of the aluminum beam pipe with a grooved surface is presented in Fig. 8.19 (b), which was made using an extrusion method. The groove is a triangle type where a tip has an angle of approximately 20° and a roundness of approximately 0.1 mm. The TiN film is subsequently applied to the grooved surface. For the copper beam pipe, the grooves are machined on a block, and the blocks are welded to the top and the bottom of the beam pipe. If the grooved surface is prepared at the top and the bottom of the beam channel, the reduction in the electron density by a factor of 4 is expected from the experiments compared to the case of plain copper beam pipe.

8.7.5 Clearing electrode

It was also reported that a clearing electrode is very useful to suppress the electron cloud [35, 79, 101−105]. The clearing electrode absorbs the electrons around the beam orbit due to a static electric field. The clearing electrode is not a novel idea and has previously been applied to proton rings [102]. The high beam impedance, however, has made it difficult to apply the method to recent high-intensity positron/proton rings. A method for forming a thin electrode on an inner surface using a thermal spray was developed in KEK [79]. The electrode has a total thickness of approximately 0.3

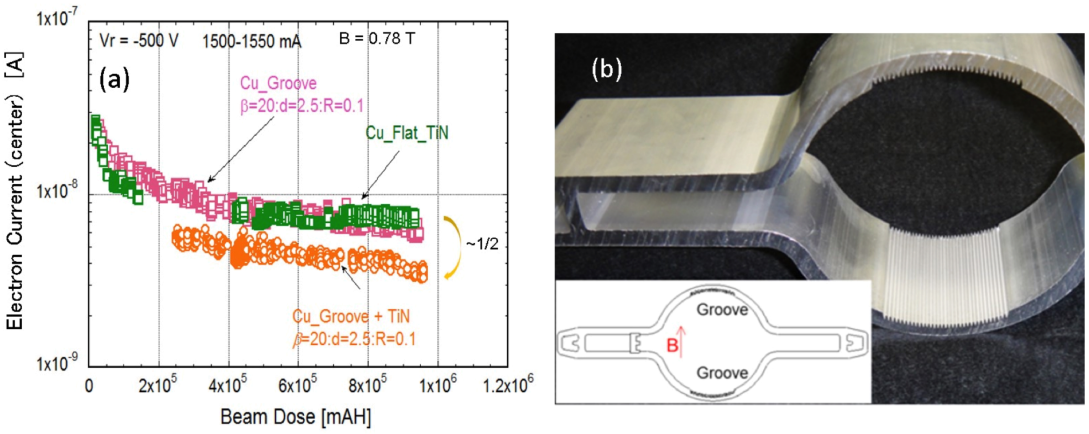

Figure 8.19: (a) Typical results of measured electron currents for a beam pipe having grooved copper surface, flat copper surface and grooved copper surface with TiN coating as a function of beam dose (time integral of beam current) installed in a wiggler section. The electron current reflects the electron density around the beam. (b) Grooved surface at top and bottom of an aluminum beam pipe with antechambers formed by a extrusion method.

mm (multiple layers of 0.2 mm aluminum ceramics and 0.1 mm of tungsten on the aluminum layer) and has a low beam impedance and a high thermal conductivity to the beam pipe compared to the conventional strip-line type.

The electrode was installed into a wiggler magnet of the KEKB positron ring and the number of electrons around the beam was measured [79]. A result is shown in Fig. 8.20 (a). A reduction in the electron density of two orders of magnitude was observed when a positive voltage greater than 300 V was applied to the electrode. For the SuperKEKB, 112 clearing electrodes are adopted in a wiggler magnet, where the beam pipe is straight and the thermal spray is easily applied. The electrode was formed on a copper block, and the blocks are welded on the top of bema pipes. Figure 8.20 (b) shows the inside view and the cross-section of the pipe with clearing electrodes. Each electrode has a length of 1.6 m and one feed-through. A positive DC voltage of **500 V** will be applied to the electrode during operation. Although the circulating beam sees the ceramic layer around the electrode (a width of approximately 4 mm), no problem was found in the experiment at the KEKB. A clearing electrode with a similar structure was installed into the CESR-TA at Cornell University and CERN, and the reduction in electron density in a wiggler magnet was verified [100, 103]. The effect of a clearing electrode were also demonstrated in DAΦNE, Italy [104, 105]

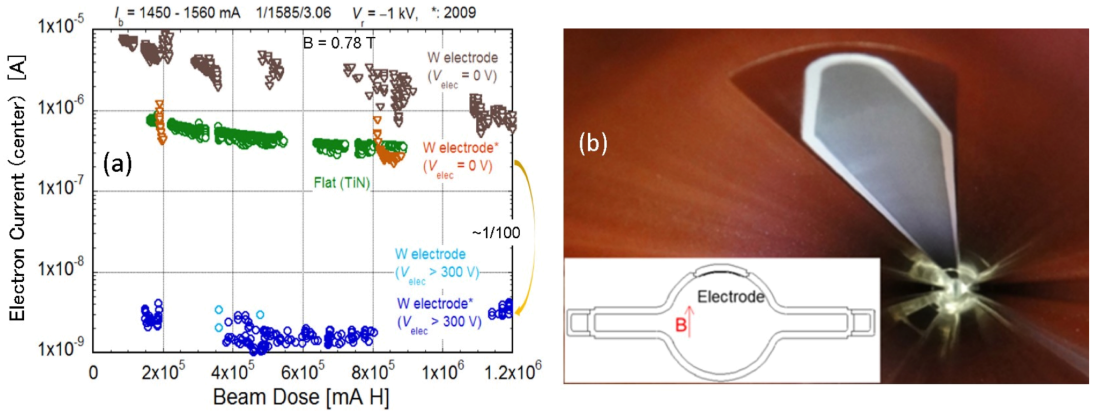

Figure 8.20: (a) Typical results of measured electron currents for a beam pipe having a flat surface with TiN coating and a clearing electrode, where applied voltages to the electrode are 0 V or + 300-500 V, as a function of beam dose (time integral of beam current) installed in a wiggler section. The electron current reflects the electron density around the beam. (b) Clearing electrode at top of a copper beam pipe with antechambers.

8.7.6 Expected electron density

The countermeasures against the ECE applied to the main sections in the LER are also summarized in Table 8.4 [80]. The circles indicate the applied countermeasures in each section. The electron densities expected in the case of circular beam pipes (copper) and those with the above countermeasures are presented in the table. Here the reduction efficiency in the electron density for Antechamber structure, TiN coating, Solenoidal magnetic filed, Grooved surface and Clearing electrode are assumed to be 1/5, 3/5, 1/50, 1/4 and 1/100, respectively, based on the experimental results obtained as described above. Ultimately, an average electron density less than our target value of 1×10^{11} (approximately 3×10^{10} including the reused regions) electrons m^{-3} is expected, and is lower than the threshold before. These mitigation techniques will be adopted in the positron damping ring of International Linear Collider, ILC [106, 107].

As indicated in Table 8.4, the electron densities are different by sections, that is, locations with different beta functions. The excitation of the electron cloud instability, therefore, should be considered taking into account the distribution of electron density along the ring. Figure 8.21 (a) and (b) show the expected electron density without (i.e., circular copper beam pipe) and with countermeasures listed in Table 8.4, and the vertical beta-function (β_y) and the product of β_y and the electron density (ρ_e) normalized by the average β_y ($<\beta_y>$) along the ring, respectively. The effect of electron

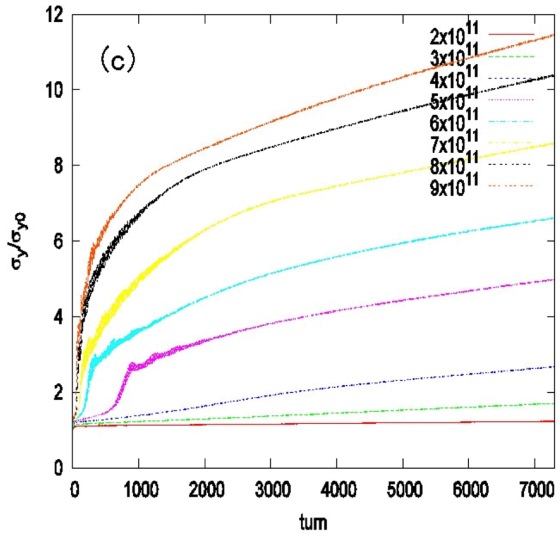

Figure 8.21: (a) Expected electron density ($n_{\rm e}$) of a circular copper pipe and a copper beam pipe with countermeasures listed in Table 8.4, (b) The vertical beta-function (β_y) and the product of β_y and the electron density (n_e) normalized by the average β_y ($<\beta_y>$) along the ring. (c) Typical simulation result for vertical beam-size blow up for several average electron densities ($\rho_{\rm e0}$) (curtsy of D. Zhou, KEK).

densities at the location with large β_y , that is, near to the collision point and the local chromaticity correction region, are higher those that at other locations. The excitation of the instability was simulated by a tracking code of PEHTS2 using the obtained distribution of electron density [108]. The result is shown in Fig. 8.21 (c), and it is found that the expected average electron density is still lower by factors than the threshold density of the instability. The further detailed study is ongoing.

8.8 TiN coating facility in KEK site

The thin TiN is coated by a sputtering of titanium rod using a magnetron discharge in an argon and nitrogen atmosphere. The coating facility is newly constructed in KEK site [36, 96]. The facility consists of 5 vertical units for Type-S and Type-Q beam pipes and 2 horizontal one for Type-B beam pipes. In the vertical unit, the beam pipes are set vertically and the titanium cathode is hung from the top of it. On the other hand, in the horizontal unit, the beam pipes are laid on stands in the solenoid coils and the titanium cathode is put on the axis of the beam channel using ceramics supports. The schematic configuration of the coating unit and the actual vertical-type coating unit are shown in Fig. 8.22 (a) and (b), respectively. In order to bake the beam pipes before

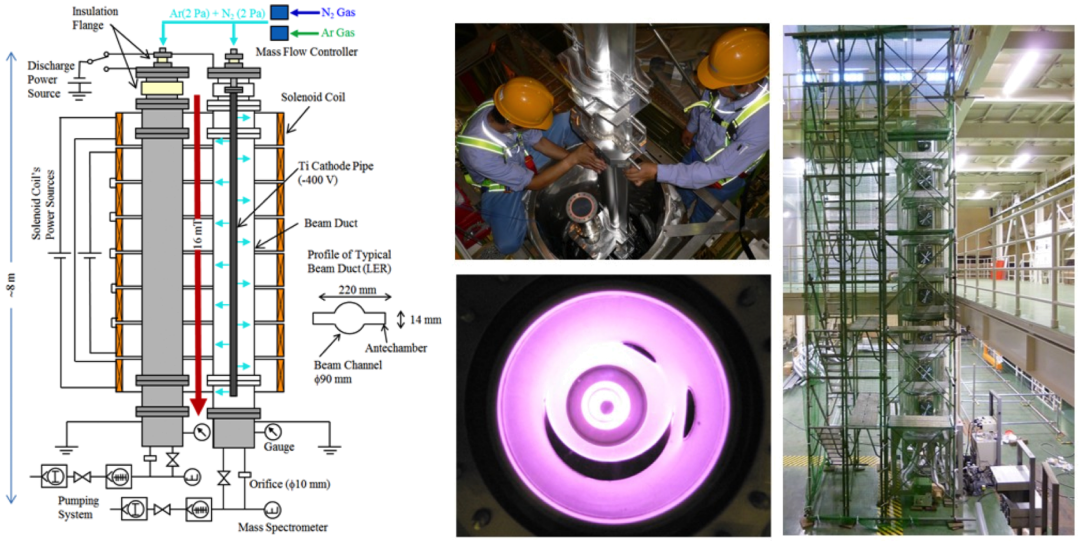

Figure 8.22: Configuration of a TiN coating unit (left) and a vertical-type unit in operation (right).

and during the coating, a baking system using hot-air circulation is incorporated in the unit. Two lines of the beam pipes are mounted side-by-side in a unit at the same time. The maximum acceptable length of beam pipe is about 5.5 m. The beam pipes are inserted in eight solenoid coils for the magnetron discharge sputtering. The pumping system consists of a turbo-molecular pump (0.3 $m^3\,s^{-1}$), a dry scroll pump (0.25 $m^3\,s^{-1}$), a flow regulating valve, a vacuum gauge and a residual gas analyzer. A titanium cathode pipe (typical outside diameter of 27.2 mm) is installed on the center axis of the beam channel and a gas inlet port is connected to it. The titanium pipe is pocked with circular holes (ϕ0.5 mm) spirally with an interval of 50 mm so that the working gases, nitrogen and argon, are supplied into the beam pipe uniformly.

In the coating process, a voltage of -400 V is applied to the titanium cathode. The strength of the solenoidal magnetic field is 16 mT. The pressures of argon and nitrogen are approximately 2 Pa in nitrogen equivalent. The temperature of the beam pipe during the coating is 130∼160 °C. The thickness of the formed TiN film is approximately 200 nm. These condition were determined from the preliminary experiment and the measurements of the SEY and the adhesion strength of the coated film [36]. The thickness of the TiN film is controlled by the coating time and the discharge current. In addition, the partial pressures, the total pressure and the discharge voltage are also monitored and continuously logged. Before the coating, the beam pipes are baked with a temperature of approximately 150 °C for over one day, and the typical

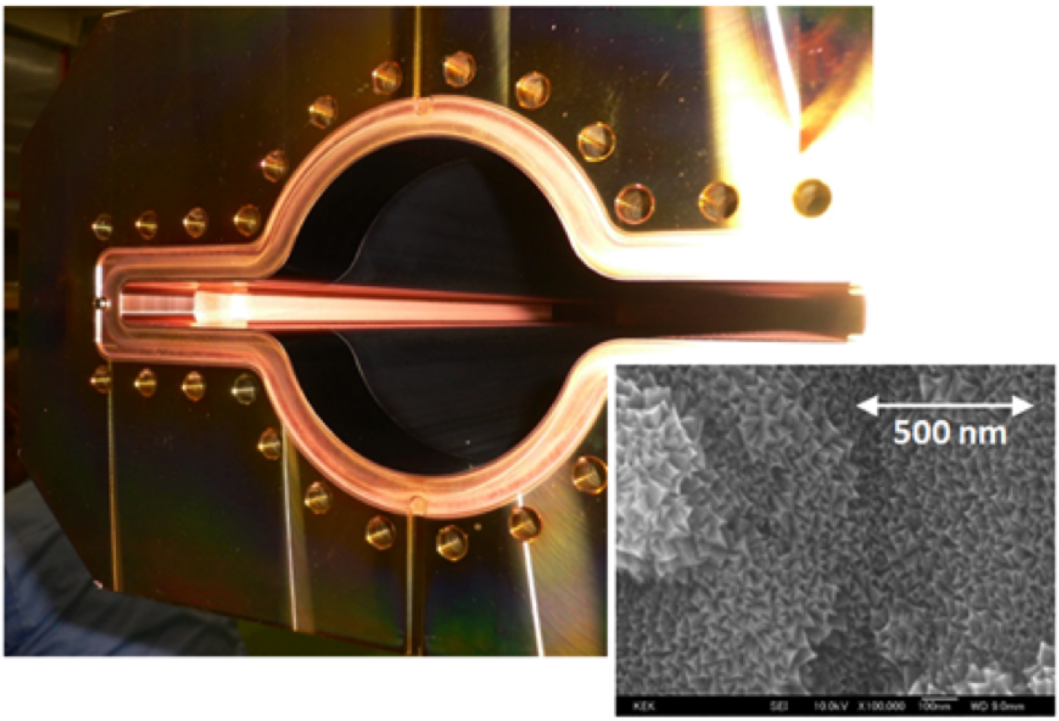

Figure 8.23: Inside view of a copper beam pipe with antechamber after coating and an electron microscopic image of the TiN coated surface.

pressure just before the coating at 150 °C is in the order of 10^{-5} Pa. Typical coating time is approximately 70 minutes. One coating process takes about 4 days including the mounting and demounting of the beam pipes.

The inside view of copper beam pipe with antechambers coated in this facility and the electron microscopic image of the TiN film formed on a sample piece are shown in Fig. 8.23. For a beam pipe with antechambers, a titanium cathode rod is installed along the beam channel, and then the coating is formed mainly on the inner surface of the beam channel. The experiment described in Sec. 7 is done using a beam pipe processed by this facility.

The SEY spectrums of the TiN films coated on a flat (red) and a grooved (blue) surfaces and uncoated flat surface (black) of aluminum sample pieces are shown in Fig. 8.24. The maximum value of the SEY of the uncoated flat surface was over 1.3 after the electron irradiation. The maximum value of the TiN films on the flat surface decreases to below 1.0 after the electron bombardment (aging). The TiN coating on a grooved surface was found to be effective to reduce the SEY further.

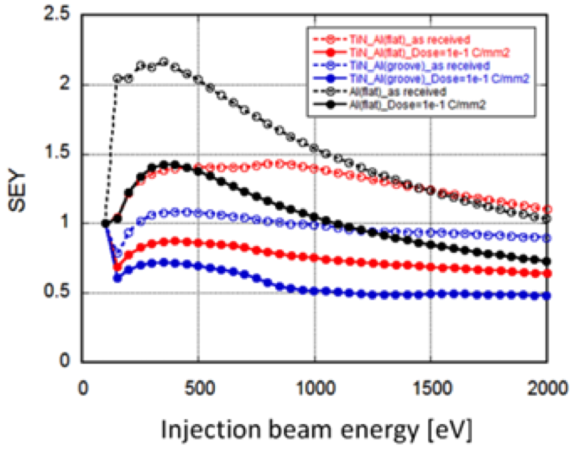

Figure 8.24: SEY spectrums of TiN films coated on a flat (red) and a grooved (blue) surfaces and uncoated flat surface (black) of aluminim samples as a function of incident electron energy.

8.9 Beam collimator

Beam collimators (or movable masks) are devices to cut off unnecessary halos of the beam and to reduce backgrounds in a particle detector [109−112]. A metal block (we call it as a jaw or a head) approached just near to the beam, and block the particles circulating away from the nominal orbit. Two types of collimators are prepared, that is, a type with the jaws approaching the beam in the horizontal direction (horizontal type) and in the vertical direction (vertical type). The locations of the collimators in the ring is shown in Fig. 8.25. In the last, newly developed 16 collimators (8 horizontal and 8 vertical types) and 13 collimators (10 horizontal and 2 vertical types) will be installed in the LER and HER, respectively. In the early commissioning phase, the KEKB-type will be reused for HER [110−112]. Described below are about the new collimators developed for the SuperKEKB.

8.9.1 Structures

Schematic drawings of the new horizontal and vertical collimators are shown in Fig. 8.26. The cross section at the both ends fit to the beam pipes with antechambers (see Sec. 1). Most of the chamber (body) and the movable jaws are manufactured from copper. In the SuperKEKB, since the main particles losses are due to the Touschek effect, the jaws are located in the both sides of the chamber (inside and outside of the ring). The jaws can be replaced with new ones in case. Tungsten, which has a high

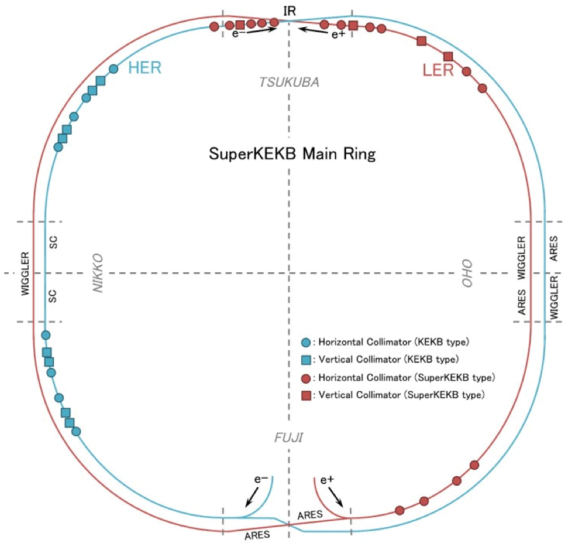

Figure 8.25: Locations of collimators for LER (red) and HER (Blue), where a rectangular and a circular symbols mean a vertical and a horizontal type, respectively.

melting point, has been adopted for a material at the tip of the jaw to avoid damages as much as possible. The length of the tip in the direction of beam is 10 mm, that is, approximately 3 times of the radiation length, which is sufficient to damp the beam hallow.

The collimator is one of the main impedance sources in the various accelerator components (see Sec. 10). Higher Order Mode (HOM) is likely excited because the beam passes through near the jaws. The beam pipe of the collimator, therefore, is tapered to decrease the impedance as much as possible, and at the same time to avoid excitations of the trapped modes [113]. Furthermore, since the width of a jaw is 12 mm, a part of the jaw can be placed behind the antechamber. This help make the low impedance while achieving the compact structure as well. The total length of a collimator is approximately 1 m. The slope at the outside of the ring also has a role to decrease the irradiated SR power density at the collimator. The inside of the antechambers in the vertical collimator is also tapered. The impedance issues arise from the collimator are discussed later.

Since there is a cavity structure behind the jaw, the components behind it could be heated and damaged by the intrusion of the HOM. RF-shield fingers, therefore, are equipped around the jaw to avoid the intrusion. The base material of the RF fingers is Inconel, which has high elasticity and annealing temperature. The finger is plated with silver with a thickness of approximately 10 μm for improving the electric contact. The silver coating works as a lubricant as well. The materials of the other contact

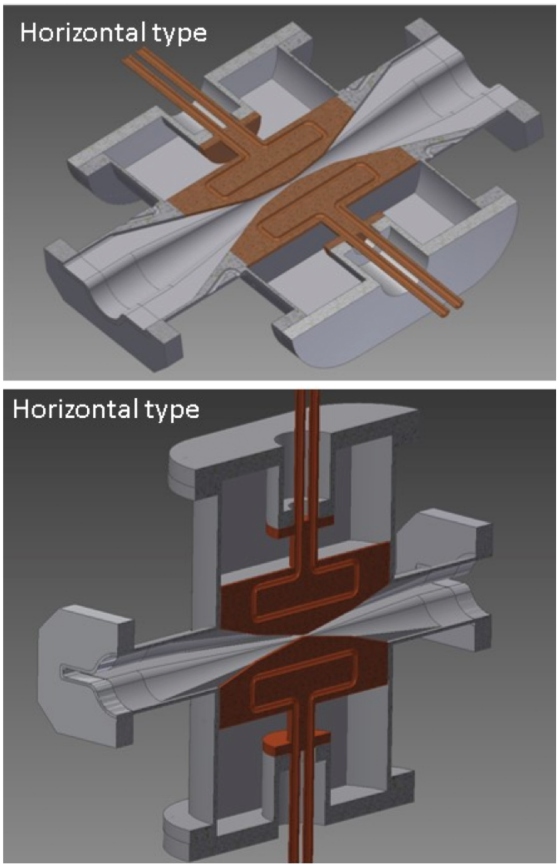

Figure 8.26: Conceptual cut model of a horizontal type (upper) and a vertical type (under) collimator for SuperKEKB.

surface will be stainless steel brazed on the copper chamber. Preparation of some hard coating on the stainless steel, such as rhodium or chrome, is in discussion.

8.9.2 Prototype

A horizontal-type collimator for test was manufactured as shown in Fig. 8.27. The jaws are driven by a 5-phase stepping motor combined with no-backlash-geared motors and no-backlash ball screws. The resolution of the linear motion in this system is 1 μm/step. A potentiometer or Linear Variable Differential Transformer (LVDT) will be adopted for the position gauge although the resistance against the radiation should be studied.

A long-duration test, which refer to shuttle the jaw back and forth for about 100 hours repeatedly in vacuum, was performed with changing the materials of the plating on the RF-shield fingers and the contact surface. The materials of the contact surface in this test are copper or stainless steel, and those of the plating are silver, rhodium or nothing. In the silver plated RF-shield fingers, the amount of the generated metallic powders was much smaller compared with the other ones.

8.9.3 HOM absorber

The beam collimators are one of the major impedance source in the ring, and the intense HOM can be generated. The intense HOM leads to excess heating or abnormal discharge of relevant components. The installation of HOM absorbers (dampers) will be indispensable near to the collimators [114−116]. Actually HOM absorbers for collimators have been installed in the KEKB and working well [116]. Research and development of the HOM absorbers are in progress. The absorbing material will be SiC or ferrite.

8.10 Impedances issues

8.10.1 Loss factors of components

In the Super KEKB, stored beam currents are high and a bunch length is short, the intense HOM can be generated at various kinds of vacuum components. For the component with a loss factor of k [V C^{-1}], the parasitic power loss, $P_{\rm l}$ [W], is calculated as

$$P_l = kqI, \tag{8.4}$$

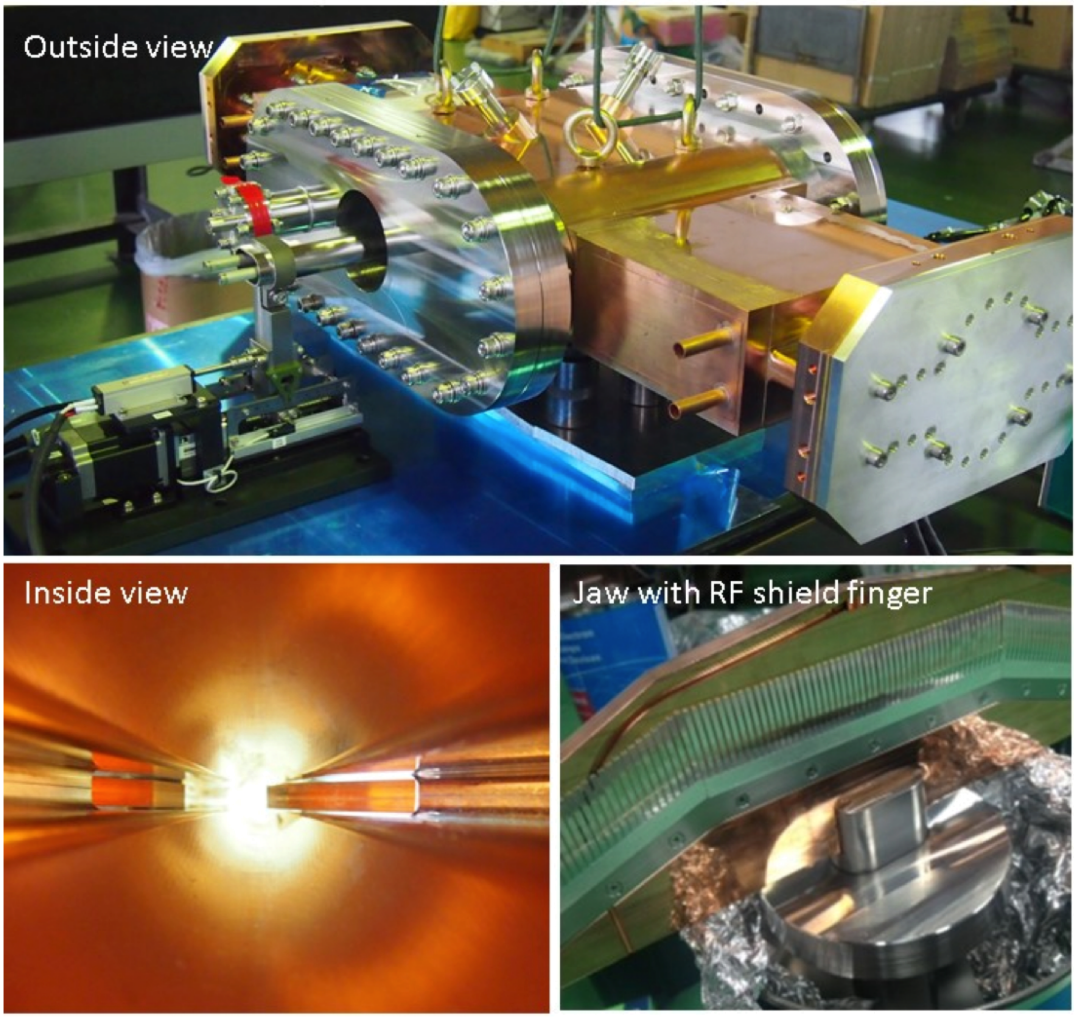

Figure 8.27: A prototype of a horizontal type collimator.

where q [C] and I [A] are the bunch charge and the beam current. For example, when the loss factor is 1 V pC^{-1}, the parasitic power loss is 52 kW for a 3.6 A beam with 2500 bunches. In designing the vacuum component, a reduced HOM design, that is, a design with long tapers in changing its cross section and with no big gaps, for example, should be widely adopted. For some vacuum components, however, HOM absorbers will be indispensable.

The loss factor of a circular beam chamber per unit length for a Gaussian bunch is given by [24]

$$k = \frac{\Gamma(3/4)c}{4\pi^2 b {\sigma_z}^{3/2}} \left(\frac{Z_0}{2\sigma}\right)^{1/2} [\mathrm{VC}^{-1}], \;\; \Gamma(3/4) \sim 1.225, \tag{8.5}$$

where c, b σ_z, Z_0 and σ refer to the speed of light (2.998×10^8 m s^{-1}), radius of beam pipe, bunch length (6 mm), impedance of vacuum (377 Ω) and conductivity of beam pipe, respectively. For the case of Super KEKB, a beam pipe with antechamber is basically used for LER and a racetrack beam pipe is mainly used for HER, but here the loss factor is roughly estimated assuming a circular beam pipe. Aluminum-alloy beam pipe ($\sigma = 3.2\times10^7$ Ω^{-1}m^{-1}.) and copper one ($\sigma = 5.9\times10^7$ Ω^{-1}m^{-1}.) are assumed for LER and HER, respectively. The loss factor for LER (b = 45 mm) and HER (b = 25 mm) are 1.1 $\times10^9$ V C^{-1} and 1.4×10^9 V C^{-1} per unit length, respectively.

A Loss factors for various vacuum components were calculated using electromagnetic field simulation code, GdfidL, Microwave studio, and so on. Table 8.5, summarizes loss factors and resultant HOM powers for major components. The largest impedance source is accelerating cavities at present. How to reduce and how to absorb the intense excited HOM is one of key issues. The second is resistive wall, and the third is bellows chambers.

The contribution of the grooved structure and the clearing electrode to the total impedance was found to be very small, partially attributable to the relatively large aperture of the beam pipes. The contribution of the loss factors, for example, is less than 2% of the total loss factor in a ring.

8.10.2 Beam collimator (LER)

The loss and kick factors of the new collimators in the bunch length 6 mm are shown in Fig. 8.28 as a function of the distance between the beam orbit and the top of jaw, d. The loss factor is approximately 0.04 V pC^{-1} per collimator for d = 10 mm, and this value is smaller than the typical value of 0.2 V pC^{-1} [7] for the KEKB type collimators. The loss factors depends on the distance, d. Assuming the positions for each collimators as shown in Table 8.6, the total loss factor is about **0.5 V pC^{-1}**, and

	Component	k [a)] [V C^{-1}] (per 1 m)	Number of Items	Total k [V C^{-1}]	P_l [b)] [kW]
LER (3.6 A)	Resistive Wall [c)]	1.1×10^{9}	3000 m	3.3×10^{12}	170
	Pumping Holes	4.3×10^{2}	2400 m	1.0×10^{6}	5.2×10^{-5}
	Flange	1.5×10^{7}	2000	3.0×10^{10}	1.6
	Bellows chamber	3.0×10^{9}	1000	3.0×10^{12}	160
	SR Mask [d)]	1.8×10^{-3}	1000	1.8×10^{3}	9.3×10^{-8}
	Gate Valves	3.0×10^{9}	47	1.4×10^{11}	7.3
	Collimators	$3.7\times10^{10*}$	13	4.8×10^{11}	26
	Taper	3.8×10^{8}	50	1.9×10^{10}	0.99
	BPM	1.6×10^{8}	450	7.2×10^{10}	3.7
	B×B FB BPM	5.9×10^{8}	10	5.9×10^{9}	0.31
	FB kicker	5.0×10^{11}	1	5.0×10^{11}	26
	Grooved surface	2.6×10^{8}	520 m	1.4×10^{11}	7.2
	Clearing electrode	1.1×10^{9}	150 m	1.7×10^{11}	8.8
	IR Chamber	8.0×10^{8}	1	8.0×10^{8}	0.041
	Cavity (ARES)	4.4×10^{11}	22	9.7×10^{12}	500
	Total			~20×10^{12}	~1000
HER (2.6 A)	Resistive Wall [e)]	1.4×10^{9}	3000 m	4.2×10^{12}	110
	Pumping Holes	7.0×10^{7}	1000	7.0×10^{10}	1.9
	Flange	3.0×10^{8}	2000	6.0×10^{11}	16
	Bellows chamber	3.0×10^{9}	1000	3.0×10^{12}	81
	SR Mask[d)]	2.5×10^{8}	1000	2.5×10^{11}	6.8
	Gate Valves	3.0×10^{9}	41	1.2×10^{11}	3.2
	Collimators [f)]	2.3×10^{11}	16	3.7×10^{12}	100
	Taper	3.8×10^{8}	20	7.6×10^{9}	0.21
	BPM	1.6×10^{8}	450	7.2×10^{10}	1.9
	B×B FB BPM	5.9×10^{8}	10	5.9×10^{9}	0.16
	FB kicker	5.0×10^{11}	1	5.0×10^{11}	14
	IR Chamber	8.0×10^{8}	1	8.0×10^{8}	0.022
	Cavity (ARES)	4.4×10^{11}	8	3.5×10^{12}	95
	Cavity (SCC)	1.4×10^{12}	8	1.1×10^{13}	300
	Total			~30×10^{12}	~800

[a)] Loss factor for $\sigma_z = 6$ mm.

[b)] Power loss

[c)] ϕ90 aluminum-alloy is assumed.

[d)] 10 mm height

[e)] ϕ50 copper is assumed.

[f)] KEKB type, a gap of 10 mm is assumed.

Table 8.5: Each loss factors, total loss factors and total power losses for main vacuum components.

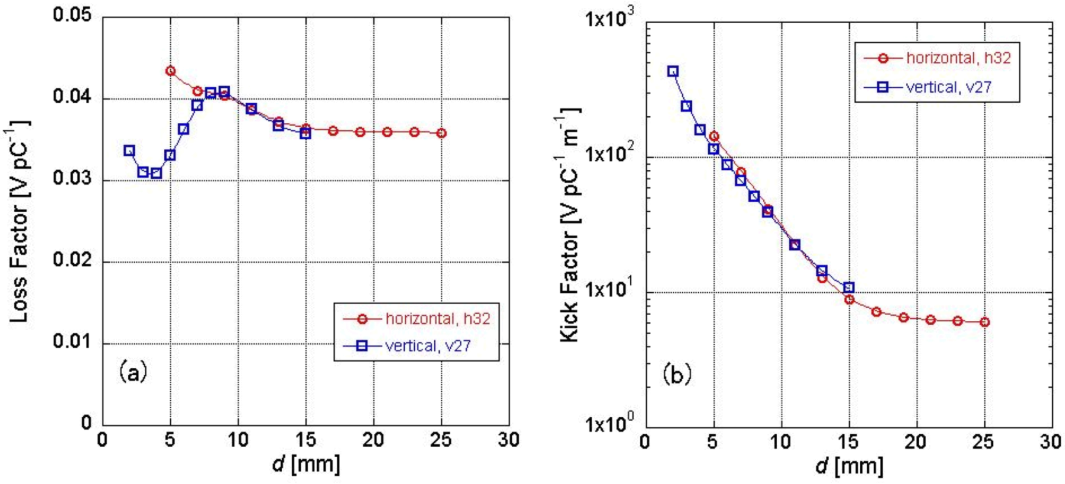

Figure 8.28: (a) Loss factors and (b) kick factors for a horizontal and a vertical type collimators as a function of the distance between the beam orbit and the jaw.

this value doesn't cause any problems in terms of the RF system.
A high kick factor in a vertical collimator in LER, however, could cause Transverse Mode Coupling Instability (TMCI). The TMCI is one of main factors to limit the bunch current, ⊥and a threshold that arises the instability is given from the following formula [117].

$$I_{thresh} = \frac{C_1 f_s E/e}{\sum_i \beta_i k_{\perp i}(\sigma_z)} \tag{8.6}$$

In this formula, C_1, f_s, E/e, β_i and k_i refer to a constant (˜ 8), the synchrotron frequency (2.43 kHz, $\nu_s = 0.0244$), the beam energy in eV (4.0 GeV), beta function at each collimator, and kick factor as a function of the bunch length(σ_z). When the apertures are set to values as shown in Table 8.6, the thresholds are 16 mA/bunch in horizontal and 1.6 mA/bunch in vertical. Thus, the design bunch current in SuperKEKB (1.44 mA) is comparable to the threshold in vertical direction. Detailed sturdy is ongoing using a beam tracking simulation, but it should be noted that the TMCI in the vertical direction can be a serious problem.
The longitudinal and transverse impedances in the horizontal and vertical collimator are calculated. There is no narrow resonance peak, which means no trapped mode, regardless of d.
A coupling between a beam and vacuum components changes the beam length because the impedance distorts the well-type potential (potential well distortion). The change of the bunch length is calculated from the following formula [118].

Collimator No. [a]	d [mm]	k [b] [V pC^{-1}]	k$_\perp$ [c] [V pC^{-1}m^{-1}]	β_x [d] [m]	β_y [d] [m]
D06 H1	-16.0 / +17.0	0.036	8	24.28	5.5043
D06 H2	-16.0 / +16.0	0.036	8	24.28	5.5042
D06 H3	-16.0 / +15.0	0.036	9	24.28	5.5043
D06 H4	-13.0 / +13.0	0.037	15	24.28	5.5042
D03 H1	-21.0 / +20.0	0.036	6	28.97	3.021
D03 H2	-18.0 / +20.0	0.036	7	28.97	3.021
D03 V1	-9.0 / +9.0	0.041	40	10.38	17.05
D03 V2	-9.0 / +9.0	0.041	40	10.38	17.05
D02 H1	-10.6 / + 12.0	0.038	25	33.20	19.06
D02 H2	-16.0 / +20.0	0.036	8	81.01	22.01
D02 H3	-18.0 / +21.0	0.036	7	31.09	173.3
D02 H4	-13.0 / +9.0	0.04	40	45.63	6.236
D02 V1	-2.0 / 2.0	0.034	450	21.79	104.6

[a] Lattice: sler_1689.disp
[b] Loss factor
[c] Kick factor
[d] Beta function at collimators

Table 8.6: Design positions of jaws (distance from the beam orbit), loss factors, kick factors of each collimator, and the beta functions of each location of it.

$$\left(\frac{\sigma_z}{\sigma_{z0}}\right)^3 - \frac{\sigma_z}{\sigma_{z0}} - \frac{\alpha I_b \mathrm{Im}\left(\mathrm{Z}_{//}/n\right)_{eff}}{\sqrt{2\pi}\,(E/e)\,\nu_{s0}^2}\left(\frac{R}{\sigma_{z0}}\right)^3 = 0 \tag{8.7}$$

In this formula, σ_{z0}, σ_{z}, α, I_b, $\mathrm{Im}(Z_{//}/n)_{\mathrm{eff}}$, E/e, ν_{s0} and R refer to the initial bunch length (6 mm), bunch length by the distortion effect, momentum compaction factor (3.18×10^{-4}), bunch current (1.44 mA), imaginary part of the effective longitudinal impedance, beam energy in eV (4 GeV), synchrotron frequency (2.43 kHz) and average radius of a ring ($3016/2\pi$ m). Since the collimators has an inductive impedance, the bunch is lengthened. The total inductance in LER is 16.3 nH, and the inductances per horizontal and vertical collimator are 1.09 nH and 1.8 nH. The distorted bunch length by the effect is calculated to 6.96 mm when the initial bunch length is 6 mm. Detailed evaluation of the potential well distortion is required using a beam tracking simulation.

8.10.3 Resistive wall instability

The wall current induced on the beam pipe extends behind the bunch due to the finite resistivity of the wall. Their electro-magnetic field can act on the charged particles arriving later and may increase their oscillation amplitude and cause instabilities in bunched beam. The longitudinal resistive wall impedance is given by [24]

$$\frac{Z_{0//}(\omega)}{n} = (1-\mathrm{sgn}(\omega)i)\frac{R}{\sigma\delta bn} = Z_0\frac{(1-\mathrm{sgn}(\omega)i)}{2}\frac{\delta}{b}\,[\Omega], \tag{8.8}$$

where σ is the conductivity of beam pipe ($\sigma = 3.2\times10^7$ $\Omega^{\text{-}1}\mathrm{m}^{\text{-}1}$ for aluminum alloy and 5.9×10^7 $\Omega^{\text{-}1}\mathrm{m}^{\text{-}1}$for copper) and $\delta = (2/\omega\mu\sigma)^{1/2}$ is the corresponding skin depth. The formula holds when n << $R\gamma/b$, where b is the radius of beam pipe, R is the average radius of storage ring ($3016/2\pi$m). Z_0 is the impedance of a vacuum (120π) and the n is the mode number (ω ˜ $n\omega_{0,}$ $\omega_0 =$ 6.25×10^5 $\mathrm{s}^{\text{-}1}$).
On the other hand, the transverse resistive wall impedance is given by [24]

$$Z_{1\perp} = Z_0(1-\mathrm{sgn}(\omega)i)\frac{\delta R}{b^3}\,[\Omega\mathrm{m}^{-1}]. \tag{8.9}$$

The transverse resistive wall impedance can drive coupled-bunch instabilities. The growth rate ($1/\tau_{\mathrm{m}}$) for the m-th mode without Landau damping is given by [119]

$$\frac{1}{\tau_m} = -\frac{eMI_bc}{4\pi\nu E}\sum_{k=-\infty}^{\infty}\mathrm{Re}Z_\perp[(kM-m+\nu)\omega_0]\,[\mathrm{s}^{-1}], \tag{8.10}$$

where M is the number of bunches (2500), I_{b} is the bunch current, ν is the transverse (vertical) betatron tune, c is the speed of light and E/e is the beam energy in eV.

For LER, $I_{\rm b} = 1.44$ mA, ν= 46.57, $E/e = 4$ GeV and $b = 45$ mm. The maximum $Z_{1\perp}$ is given at $m = 47$ and $k = 0$, i.e.,

$$\omega = (-47 + 46.57)\omega_0 = -0.43\omega_0 = -2.69 \times 10^5 \ {\rm s}^{-1}. \ ({\rm f} = 4.28 \times 10^4 \ {\rm Hz}). \qquad (8.11)$$

Then, δ is 430 μm. Note here that the skin depth at the corresponding frequency is so thick that coatings with a thickness of a few μm will have negligible effect on the instability. The growth rate is calculated as

$$\frac{1}{\tau_{47}} = \frac{3.6 \times 3 \times 10^8}{4\pi \times 46.57 \times 4.0 \times 10^9} \times 120\pi \times \frac{4.3 \times 10^{-4} \times 480}{(45.0 \times 10^{-3})^3} = 3.9 \times 10^2 \ [{\rm s}^{-1}], \qquad (8.12)$$

or

$$\tau_{47} = 2.5 \times 10^{-3} \ [{\rm s}]. \qquad (8.13)$$

For HER, the τ_{44} of 1.3×10^{-3} [s] is obtained for $I_{\rm b} = 1.04$ mA, ν= 43.57 and $E/e = 7$ GeV, $b = 25$ mm and $\delta = 317$ μm.
As a result, the instability can be suppressed by a feed-back system since the response frequency is about 10 kHz.

8.10.4 Microwave instability

An increase in bunch current can lead to longitudinal instabilities of a single bunch. Since it is often accompanied by high-frequency signals, it is called as a microwave instability. The instability increases the emittance, the bunch length and the energy spread. The Coherent Synchrotron Radiation (CSR) is generated when a bunch traverse a dipole field, and it is reported that the CSR can cause heavy microwave instability [27, 28]. The instability is important for LER since the bunch charge is high and the energy is low.
The longitudinal wakes of various vacuum components, such as resistive wall with TiN coating, bellows chambers, flange gaps, CSR and so on, are calculated for a beam pipe with antechambers as shown in Fig. 8.1 (a), where the radius of beam channel is 45 mm. The highest peak was given by the CSR in arc. The increase in the bunch length and the energy spread was estimated using a particle tracking code. The preliminary result is shown in Fig. 8.29 [108]. It was found that the increases in the bunch length and the energy are small at the design bunch current (8×10^{10} positrons/bunch) and the microwave instability has no problem. The further detailed studies are in progress.

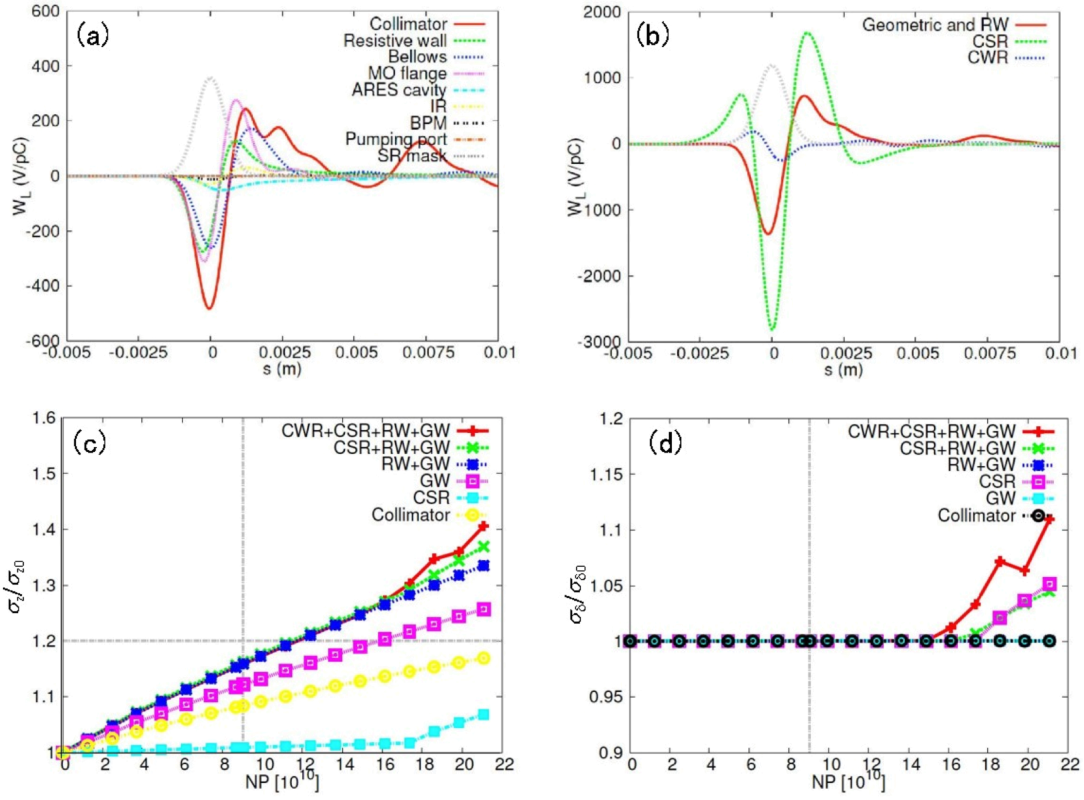

Figure 8.29: (a) (b) Wake functions of vacuum components including that of CSR for $\sigma_z = 0.$ 5 mm used in the simulation. CSR, CWR and RW mean the coherent synchrotron radiation, the CSR in wiggler section and the resistive wall. Increase in (c) the bunch length (σ_z/σ_{z0}) and (d) the energy spread ($\sigma_\delta/\sigma_{\delta 0}$) due to the microwave instability as a function of bunch charge. GW means the geometrical wake.

8.10.5 Incoherent tune shift

Generally, noncircular beam pipes induces the incoherent tune shift due to the quadrupole component in the resistive-wall wake field [25]. For the case of KEKB HER, where a beam pipe with race-track shape was used (see Fig. 8.1 (d)), a tune shift of approximately 0.03 was observed in both the horizontal and vertical direction per 1 A beam. In the SuperKEKB, since the stable tune area is not so large, the large change of tune during beam injection is undesirable. New beam pipes for HER arc sections have antechambers as shown in Fig. 8.1 (b), and the large tune shift is expected. Since the quadrupole component induced by the wall current causes the tune shift, it is expected that an elliptical beam channel can help to decrease the quadrupole component by compensating the aperture of antechambers. The electric filed around the beam was calculated by MAFIA code, and the intensity of quadurpole component is evaluated by changing the ellipticity of beam channel, that is, the ratio of vertical radius (major radius, $r_{\rm y}$) and horizontal radius (minor radius, $r_{\rm x}$) of the beam channel [26]. Figure 8.30 (a) shows the dependence of the tune shift as a function of the ellipticity ($r_{\rm y}/r_{\rm x}$) for the cases of $r_{\rm y} = 50$ mm. The height of antechambers are fixed to 14 mm. The horizontal or vertical tune shifts are almost zero when the ellipticity of approximately 0.86. For comparison, it was found that there is no solution for the case of $r_{\rm y} = 40$ mm. Figure 8.30 (b) is a contour plot of the intensity of electric field in the beam pipe. The circular contour lines around the center of beam channel mean the small quaduruple component there. Based on the result, a beam channel with $r_{\rm y} = 25$ mm and $r_{\rm x} = 22$ mm is finally adopted to the present design. The expected maximum tune shift is less than 0.1. In the case of $r_{\rm y} = 45$ mm, as a beam pipe for LER as shown in Fig. 8.1 (a), it was found that the expected tune shift is sufficiently small even for the circular beam channel, and the elliptical cross section is unnecessary. The elliptical beam channel can be formed during the cold drawing process.

8.11 Preprocessing before installation

In the SuperKEKB, more than 1200 beam pipes will be replaced with new ones. All new beam pipes are pre-baked before the installation into the ring in order to remove contamination on the inner surface, and to check the ultrahigh-vacuum property. In addition, almost all the beam pipes for LER are coated with thin TiN to mitigate the ECE as described before. A preprocessing facility with 7 coating units and 4 baking units are constructed in KEK site. The whole view of the facility is shown in Fig. 8.31. Please see Sec. 8 for the TiN coating facilities.

The flow chart of the pre-installation process is presented in Fig. 8.32. First of all, the

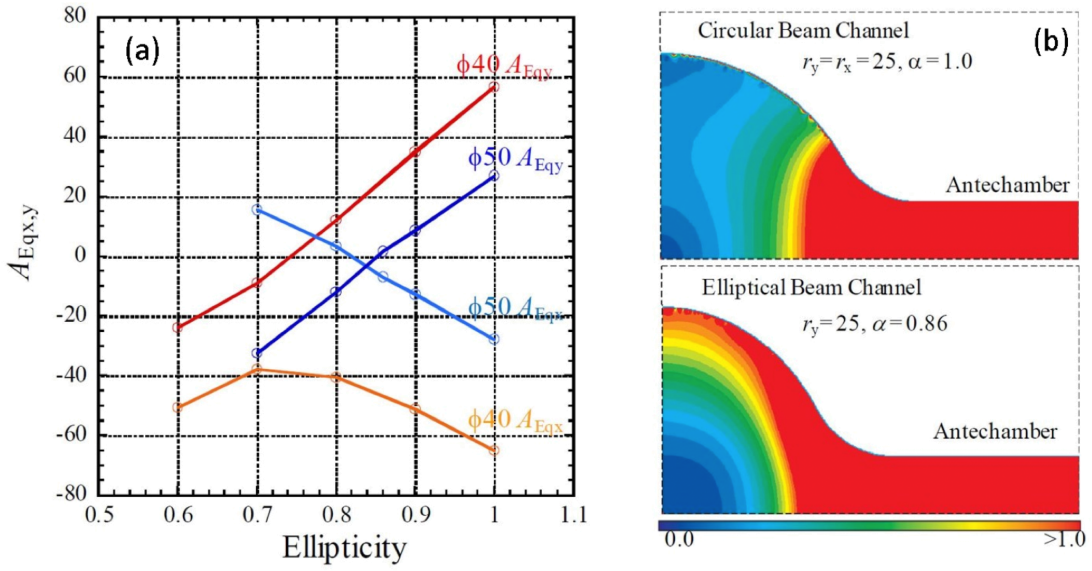

Figure 8.30: (a) Change of the incoherent tune shift by the ellipticity (α) of beam channel, r_y/r_x, where r_y and r_x mean the vertical and horizontal radius of the beam channel, respectively, for $r_y = 25$ mm. (b) Contour plot of the absolute value of wake field induced by the resistive wall for a circular beam channel and an elliptical beam channel, were $r_y = 25$ mm and $\alpha = 0.86$.

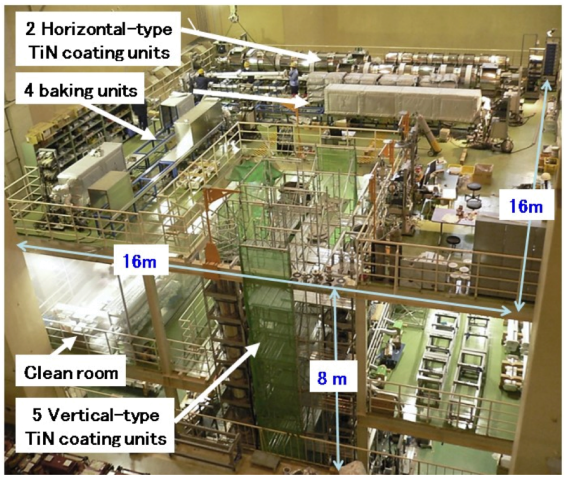

Figure 8.31: Whole view of the preprocessing facility consisting of 5 vertical-type and 2 horizontal-type TiN coating units, and 4 baking units constructed in KEK site.

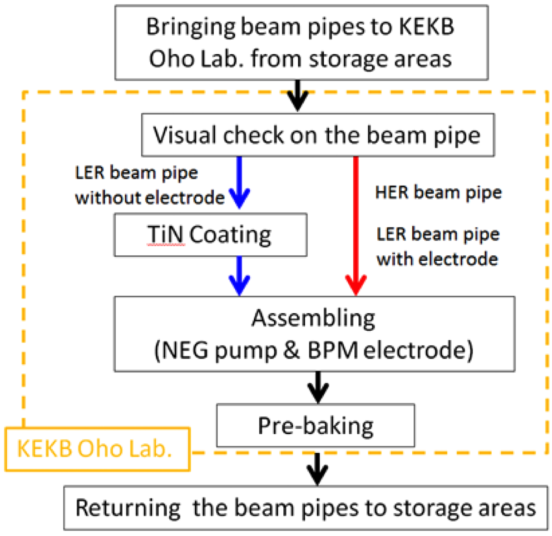

Figure 8.32: Flow chart of pre-installation procedure.

beam pipes are transported to the facility from the storage house. They are visually checked in a clean room, and if there are any problems like contamination of the inner surface, burr at BPM ports etc., they are properly treated in this stage. Then, for the beam pipes of the LER, the beam pipes are coated with TiN in principle. In the next step, the pumps assembled to the beam pipe in a clean room. The beam pipes are then baked followed by filling them with dry nitrogen supplied from the liquid nitrogen. Finally, the beam pipes are returned to the storage house, and waiting for the installation into the ring.

The baking facility consist of 4 baking units in which a hot-air heating method is employed (Fig. 8.33). Two lines of the beam pipes are mounted up and down in a hot-air oven surrounded by a thermal insulating sheets. The beam pipes can be heated up to 150 °C within 2 hours. One unit has two pumping systems, and each consists of a turbo-molecular pump (0.3 $m^3 sec^{-1}$), a dry scroll pump (250 L min^{-1}), a cold cathode gauge and vacuum gauges (Extractor gauge). A few vacuum systems have a residual gas analyzer to monitor the quality of the vacuum after the baking. The unit can bake the beam pipe with a length up to 5.2 m. Several short beam pipes will be connected and can be baked at the same time to increase the working efficiency.

The beam pipes are baked typically at 150 °C for 26 hours. The installed NEG pumps are activated in parallel during the baking of beam pipes. The power of heaters for NEG activation is kept at 50 % during the baking. The power is increased up to 90 % at the final stage, and kept for 30 minutes. One baking process takes about three

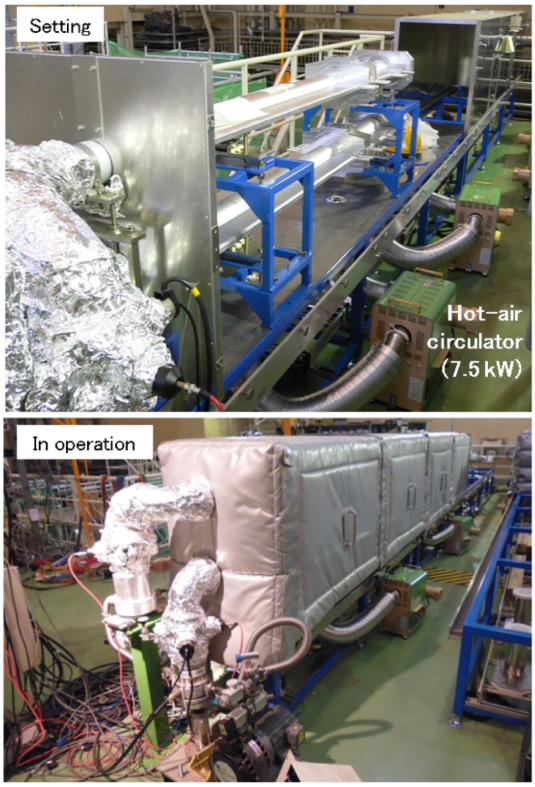

Figure 8.33: Baking unit utilizing hot-air circulation system.

days. The goal pressure after the baking is below 1×10^{-7} Pa [7]. Approximately 10 persons work for the pre-installation process. The expected weekly output will be 10 - 15 pipes in average.

8.12 Infrastructures and facilities

The vacuum components, such as beam pipes, bellows chambers, etc., are cooled with pure water all around the ring. The total SR powers of LER and HER are approximately 7.4 MW and 6.3 MW (see Table 8.1), respectively. Considering a dissipated power from HOM all over the ring, the power absorbed by beam pipes will increase further (˜1 MW per ring, see Table 8.5). On the other hand, the KEKB cooling capacity was about 8 MW in total for vacuum system, which was almost the same as the total SR power expected in the KEKB. Therefore, the increase of cooling capacity by a factor of 2 is indispensable for the SuperKEKB, especially for the wiggler section in both rings. Figure 8.34 shows the total power loss at four arcs and four straight

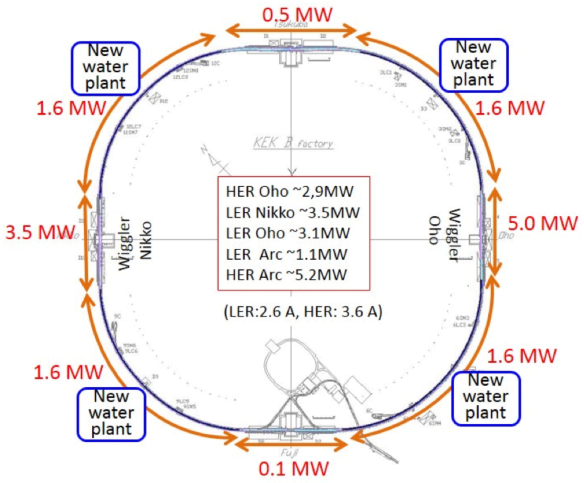

Figure 8.34: Distribution of heat loads to beam pipes due to SR and the parasitic loss along a ring, where the locations of four new water plat are also indicated.

sections along the tunnel. High cooling power is required for Oho and Nikko straight sections, where the wiggler sections are located. In order to increase the cooling power, four new cooling plants are constructed on the ground near to the arc sections in addition to the existing four plants at straight sections. The flow rate of these eight cooling plants are summarized in Table 8.7.

The temperature of water is kept at approximately 25 ± 1 °C at the entrance of beam pipes. The average flow rate is about 20 L min^{-1} along the beam pipe for a cooling pipe with 15A size (diameter of 1/2 inches). The new beam pipes for LER has two cooking channel at the both sides of beam pipes as described above. The length of one cooling loop in the tunnel and the layout of the loop should also be optimized. For example, if one cooling loop has a length of about 10 m in the tunnel, the average dissipated power for 10 m is about 30 kW. Then the temperature rise for one loop reaches up to 21 °C ($= 30 \times 10^3/70/20$).

Because the dissipation of SR power is concentrated in the wiggler section and the section downstream from it. A flow rate should be increased up to approximately 120 L min^{-1} to absorb the high SR power there. The pressure drop between the inlet and outlet valve should be about 0.8 MPa or less to realize the flow rate. So, a header system is prepared for the wiggler sections. The water flow is divided into 9 loops at a maximum. The pipe size of inlet valve is increased from existing 25A (1 inche) to 32A (1 1/4 inches) or 40A (1 1/2 inches).

The main water pipes for the HER and the LER are made of copper and aluminum, respectively, and stainless steel connectors and short pipes are used to avoid the electric

		KEKB		SuperKEKB	
		Flow rate (L min^{-1})	ΔT [a] (25 - 35)	Flow rate (L min^{-1})	ΔT [a] (25 - 45)
Existing Facilities	Tsukuba	1800	10.0	1800	20.0
	Oho	1800	10.0	1800	20.0
	Fuji	1800	10.0	1800	20.0
	Nikko	1800	10.0	1800	20.0
New Facilities	North			1700	20.0
	East			1700	20.0
	South			1700	20.0
	West			1700	20.0
Total		7200		14000	

[a] Rise in temperature

Table 8.7: Flow rates of existing and new cooling plants.

erosion between aluminum and copper. The cooling water is deoxidized pure water. The gasket at the flanges are made of carbon made of expanded graphite, which has a high resistance to radiation.

The gate valves are actuated by a compressed air. The compressed air system will be reused in the SuperKEKB. Two compressors on the ground supply the compressed air in whole of the ring. The pressure is 0.9 MPa at the outlet of the compressor, but it decreased to 0.6 MPa in the tunnel. The compressor has a drain to remove the humid. In the future, a dry nitrogen system will be prepared to make vacuum system maintenance easier in the tunnel. The nitrogen will be supplied from liquid nitrogen stored in a refrigerator system on the ground.

Electric power plugs, that is, AC 200 V and 100 V, will be prepared in the tunnel for in situ rough pumping, welding, and controls.

8.13 Commissioning

A procedure of the vacuum start-up in the tunnel is as follows:

(1) A portable rough pumping system consisting of a scroll type dry pump (250 L min^{-1}), a turbo molecular pump (0.3 m^3 s^{-1}) is attached to a pumping port with an L-angle valve. The pumping port are every 40 m along the ring.

(2) After rough pumping, the high voltage is applied to CCG and ion pumps in

the corresponding sector.

(3) Ion pumps are baked using the built-in heaters for approximately 1 day.

(4) NEG pumps are activated with the pattern operation for approximately one day. The baking of ion pumps finish 1−2 hours after starting NEG activation.

(5) The L-angle valve for the roughing pump is closed just after the NEG activation. The decrease of pressure is checked for one day at least.

(6) The rough pumping system is removed.

When any work to break vacuum is required, in reverse, a dry nitrogen is introduced through a pumping port with L-angle valve described above, after checking the closed status of gate valves at the ends of the corresponding sector and also the off status of CCG and ion pumps. If the work is minimal one, the dry nitrogen is kept flowing even during the work in order to avoid the absorption of water on the surface. The starting up follows the procedure described above, but the baking and the NEG activation time are adjusted by condition.

As is well known the photo-desorption rate, η [molecules photon^{-1}], decreases with beam operation time, that is, a photon dose [photons m^{-1}] [5, 55 - 61]. Figure 8.35 shows the decrease in η in arc sections measured in the KEKB HER as a function of beam dose [mA hours] or photon dose [photons m^{-1}], where a linear pumping speed of 0.03 m^3 s^{-1} m^{-1} is assumed [9]. At the photon dose of approximately 1×10^{25} photons m^{-1}, the η reached down to 1×10^{-6} molecules photon^{-1}, that is, the design value. It should be noted that the η seems still decreasing further in this figure. From the experience in KEKB, it actually takes a few years to achieve the η of 1×10^{-6} molecules photon^{-1}from the beginning of beam operation.

Here the frequency of the NEG activation at a steady state (i.e., in operation at the design current) is roughly estimated, assuming an η of 1×10^{-6} molecules photon^{-1} [69]. Since the linear photon density at a full current is approximately 6×10^{18} photons s^{-1} m^{-1} (see Table 8.1), the gas desorption rate is 2 $\times10^{-8}$ Pa m^3 s^{-1} m^{-1} (300 K). If the main gas component is CO, the pressure just after an activation is then approximately 1.6×10^{-7} Pa. The timing of the re-activation will be determined by the beam life time, the background to the detector, and so on. Here we assume that the NEG is activated when the pressure goes up to 1.0×10^{-6} Pa, where the beam lifetime determined by the gas scattering is still longer than that determined by the dynamic beam aperture. In this pressure, the effective linear pumping speed along the beam pipe is approximately 0.022 m^3 s^{-1} m^{-1}, that is, the pumping speed for the NEG surface is approximately 0.32 m^3 s^{-1} m^{-2}. From the data in the ST707 Catalogue [63], the absorbed gas quantity giving this pumping speed is approximately 0.5 Pa m^3 m^{-2}

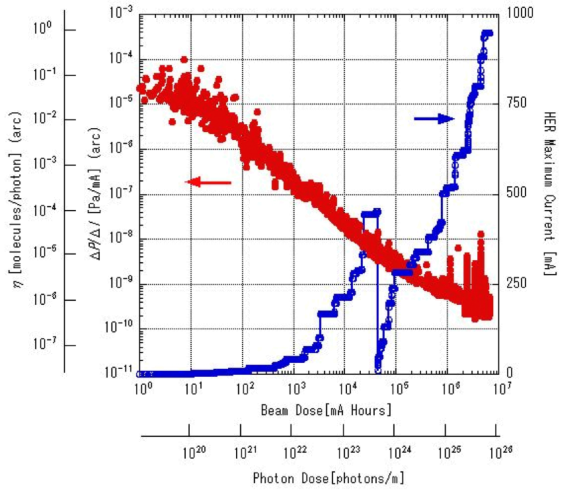

Figure 8.35: Photo-desorption coefficient, η, and the pressure rise, $\Delta P/\Delta I$ as a function of photon dose (time integral of photon flux) and a beam dose (time integral of beam current) for the KEKB HER.

for the NEG surface, that is, 0.04 Pa m^3 m^{-1} along the beam pipe. Therefore, the interval between activations are approximately 1.8×10^6 s = 21 days. Activation will be required approximately every month for continuous full-current operation.

Bibliography

[1] http://www-superkekb.kek.jp/.

[2] K. Akai et al., Proc. IPAC2012, New Orleans, May 20 - 25 (2012) 1822.

[3] Y. Funakoshi et al., Proc. PAC2010, Kyoto, June 23 - 28 (2010) 2372.

[4] Y. Ohnishi et al., Prog. Theor. Exp. Phys. (2013) 03A011.

[5] H. Hisamatsu et al., Vacuum, 47 (1996) 601.

[6] K. Kanazawa et al., Appl. Surface Sci. 169 - 170 (2001) 715.

[7] K. Kanazawa et al., App. Surface Sci., 169 - 170 (2001) 720.

[8] K. Kanazawa et al., Nuc. Instrum. Method-P.R. A499 (2003) 66.

[9] Y. Suetsugu et al., J. Vac. Sci. Technol., A21 (2003) 1436.

[10] K. Kanazawa et al., Prog. Theor. Exp. Phys. (2013) 03A005.

[11] K. Akai et al., Nucl. Instrum. Method.-P.R. A 499 (2003) 191.

[12] T. Abe et al., Prog. Theor. Exp. Phys. (2013) 03A010.

[13] T. Abe et al.,, Prog. Theor. Exp. Phys. (2013) 03A001.

[14] Y. Suetsugu et al., J. Vac. Sci. Technol., A30 (2012) 31602.

[15] K .Ohmi and F. Zimmermann, Pys. Rev. Letters, 85 (2000) 3821.

[16] H. Jin and K. Ohmi, Presented in ECLOUDf10, Cornell University, October 8-12, 2010.

[17] Y. Susaki and K. Ohmi, Proc. IPAC2010, Kyoto, June 23–28 (2010) 1545.

[18] S. Kato et al., Appl. Surface Sci., 169-170 (2001) 732.

[19] D. Hunt et al., Proc. PAC1995, Dallas, May 1-5 (1995) 2067.

[20] Y. Suetsugu et al., Nucl. Instrum. Method-P.R., A538 (2005) 206.

[21] Y. Suetsugu et al., Proc. EPAC2006, Edinburgh, June 26-30 (2006) 1438.

[22] Y. Suetsugu et al., Vacuum, 84 (2010) 694.

[23] K. Shibata, et al., Proc. 7th Annual Meeting of Particle Accelerator Society of Japan, Himeji, August 4-6 (2010) 442.

[24] A. W. Chao, gPhysics of Collective Beam Instabilities in High Energy Acceleratorsh, John Wiley & Sons, Inc. (1993) p.71.

[25] A. Chao et al., Phys. Rev. Spec. Top. - Acc. Beam. 5 (2002) 111001.

[26] K. Shibata et al., Proc. 5th Annual Meeting of Particle Accelerator Society of Japan, Higashi Hiroshima, August 6-8 (2008) 676.

[27] T. Agoh and K. Yokoya, Phys. Rev. Spec. Top. - Acc. Beam. 7 (2004) 054403.

[28] K. Oide et al., Proc. PAC2009, Vancouver, May 4-8 (2009) 23.

[29] SuperKEKB Task Force, KEK Report No. 2004-4 (2004).

[30] Y. Ohnishi and H. Sugimoto, private communication.

[31] H. J. Halama and C. L. Foerster, Vacuum, 42 (1991) 185.

[32] H. Ishimaru et al., J. Vac. Sci. Technol., A4 (1986) 1762.

[33] K. Kanazawa et al., Osaka, December 12 - 14 (1989) 118.

[34] T. Sanami, private communication. (Presented in KEKB Review committee)

[35] For example, reports presented in ECLOUDf02, CERN, April 15-18, (2002); ECLOUDf04, Napa, April 19-23 (2004); ECLOUDf07, Daegu, April 9-12 (2007); ECL2 Workshop, CERN, February 28 - March 2 (2007); ECLOUDf10, Cornell University, October 8-12 (2010).

[36] K. Shibata et al., Proc. EPAC2008, Genoa, June 23-27 (2008) 1700.

[37] AMAX Copper, Inc. gA Survey of Properties & Applications: OFHCh (1974), p.19.

[38] T. Mori et al., Proc. IPAC2012, New Orleans, May 20-25 (2012) 2035.

[39] T. Mimashi et al., Proc. IPAC2010, Kyoto, June 23-28 (2010) 1378.

[40] J. W. Flanagan et al., Proc. PAC2003, Portland, May 12-16 (2003) 2503.

[41] J. W. Flanagan et al., Proc. IPAC2010, Kyoto, June 23-28 (2010) 966.

[42] A. Novokhatski et al., Proc. EPAC2008, Genoa, June 23-27 (2008) 1664.

[43] H. Matsumoto and M. Ohtsuka, Proc. 24th Linear Accelerator Meeting in Japan, Sapporo, July 7-9 (1999) 271.

[44] Y. Suetsugu et al.,hh, J. Vac. Sci. Technol., A 27 (2009) 1303.

[45] H. Matsumoto et al., Proc. EPAC2006, Edinburgh, June 26-30 (2006) 753.

[46] W. Unterlerchner, Vacuum, 41 (1990) 1920.

[47] J. R. Chen and Y. C. Liu, Vacuum, 44 (1993) 545.

[48] Y. Suetsugu et al., Rev. Sci. Instrum., 67 (1996) 2796.

[49] Y. Suetsugu et al., Vacuum, 47 (1996) 629.

[50] Y. Suetsugu et al., Phys. Rev. Spec. Top. - Acc. Beam, 6 (2003) 103201.

[51] Y. Suetsugu et al., Proc. 14th Symp. on Acc. Sci. Technol., Tsukuba, November 11-13 (2003) 37.

[52] Y. Suetsugu et al., Rev. Sci. Instrum., 78 (2007) 043302.

[53] K. Kanazawa et al., KEK Report 90-24 (1990) 117.

[54] Kaneyasu et al., Proc. 8th Annual Meeting of Particle Accelerator Society of Japan, Tsukuba, August 1-3 (2011) 474.

[55] O. Gr?bner et al., Proc. EPAC1992, Berlin, March 24-28 (1992) 132.

[56] T. Kobari et al., J. Vac. Sci. Technol., A12 (1995) 585.

[57] S. Ueda et al., Vacuum, 41 (1990) 1928.

[58] Y. Hori and M. Kobayashi, J. Vac. Sci. Technol., A12 (1994) 1644.

[59] Y. Suetsugu and K. Kanazawa, Proc. PAC1993, Washington D.C., May 17-20 (1993) 3860.

[60] O. Gröbner et al., J. Vac. Sci. Technol., A12 (1994) 846.

[61] C. L. Foerster et al., J. Vac. Sci. Technol., A13 (1995) 581.

[62] S. Sakanaka et al., Jpn. J. Appl. Phys., 27 (1988) 1031.

[63] Technical specification of “ST707/CTAM/30D Strip (Doc. Nr. M.F140.0021.21, Rev.0)”, SAES Getters SpA., Italy, 1994.

[64] C. Benvenuti and F. Francia, J. Vac. Sci. Technol., A8 (1990) 3864.

[65] S. Yokouchi et al., Proc. EPAC1990, Nice, June 12-16 (1990) 1332.

[66] P. Chiggiato and R. Kersevan, Vacuum, 60 (2001) 67.

[67] C. Benvenuti et al., Vacuum, 50 (1998) 57.

[68] C. Benvenuti et al., Vacuum, 60 (2001) 57.

[69] Y. Suetsugu et al., Nucl. Instrum. Method, A 597 (2008) 153.

[70] http://www.aps.anl.gov/epics/.

[71] http://www.ni.com/compactrio/.

[72] https://www.yokogawa.co.jp/rtos/Products/rtos-prdcpu9-ja.htm/.

[73] H. Hisamatsu et al., J. Vac. Society of Japan, 35 (1992) 579.

[74] K. Kanazawa et al., Proc. PAC2005, May 16?20, Knoxville (2005)1054.

[75] K. Ohmi, KEK Preprint 2005-100 (2006).

[76] Y. Suetsugu, Proc. PAC2001, Chicago, May June 18 - 22 (2001) 2183.

[77] Y. Suetsugu et al., Nucl. Instrum. Method, A578 (2007) 470.

[78] Y. Suetsugu et al., Nucl. Instrum. Method, A604 (2009) 449.

[79] Y. Suetsugu et al., Nucl. Instrum. Method, A598 (2008) 372.

[80] Y. Suetsugu, Presented in ECLOUDf10, Cornell University, 8-12 October, 2010.

[81] Y. Suetsugu et al., J. Vac. Sci. Technol., A21 (2003) 186.

[82] O.Gröbner, LHC Project Report 127 (1997).

[83] O. Gröbner, Proc. 10th International Conference on High Energy Accelerators, Protvino, July 11-17 (1997) 277.

[84] Y. Funakoshi, et al., Proc. EPAC2006, Edinburgh, June 26-30 (2006) 610.

[85] Y. Cai et al., Proc. PAC2003, Portland, May 12-16 (2003) 350.

[86] B. Henrist et al., App. Surface Sci., 172 (2001) 95.

[87] A. Rossi, Presented in ECLOUDf04, Napa CA, April 19-23 (2004).

[88] K. Kennedy et al., Proc. PAC1997, Vancouver, May 12 - 16 (1997) 3568.

[89] Y. Suetsugu et al., Nucl. Instrum. Method? P.R., A554 (2005) 92.

[90] Y. Suetsugu et al., Nucl. Instrum. Method?P.R., A556 (2006) 399.

[91] C. Y. Vallgren et al., Proc. IPAC2011, San Sebastian, September 4-9 (2011) 1587.

[92] C. Y. Vallgren et al., Proc. IPAC2011, San Sebastian, September 4-9 (2011) 1590.

[93] C. Y. Vallgren et al., Proc. IPAC2010, Kyoto, June 23-28 (2010) 2033.

[94] J. R. Calvey et al., Proc. IPAC2011, San Sebastian, September 4-9 (2011) 796.

[95] M. A. Palmer et al., Proc. IPAC2010, Kyoto, June 23-28 (2010) 1251.

[96] K. Shibata et al., Proc. 4th Annual Accelerator Meeting in Japan, Wako, August 1-3 (2007) 209.

[97] A. A. Krasnov, Vacuum, 73 (2004) 195.

[98] M. Pivi et al., J. Appl. Phys., 104 (2008) 104904.

[99] J. R. Calvey et al., Proc. IPAC2011, San Sebastian, September 4-9 (2011) 796.

[100] J. Conway et al., Proc. PAC2011, New York, March 28 - April 1 (2011) 1250.

[101] L. F. Wang et al., Phys. Rev. Spec. Top. - Acc. Beam. 7 (2004) 034401.

[102] S. Bartalucci et al., Proc. PAC1987, Washington D.C., March 16-19 (1987) 1234.

[103] E. Mahner et al., Proc. EPAC2008, Genoa, June 23-27 (2008) 1655.

[104] D. Alesini et al., Proc. IPAC2010, Kyoto, June 23-28 (2010) 1515.

[105] D. Alesini et al., Proc. IPAC2012, New Orleans, May 20-25 (2012) 1107.

[106] M. T. F. Pivi et al., Proc. IPAC2011, San Sebastian, September 4-9 (2011) 1063.

[107] J. V. Conway et al, Proc. IPAC2012, New Orleans, May 20-25 (2012) 1960.

[108] D. Zhou, private communication.

[109] J. Seeman et al., Proc. EPAC2000, Vienna, June 26-30 (2000) 2298.

[110] Y. Suetsugu et al., Proc. PAC2001, Chicago, June 18-22 (2001) 2186.

[111] Y. Suetsuguet al., Rev. Sci. Instrum., 74 (2003) 3297.

[112] Y. Suetsugu et al., Nucl. Instrum. Method, A513 (2003) 465.

[113] I. Zagorodnov, et al., EUROTeV-Report-2006-074.

[114] T. Kageyama et al., Proc. EPAC1996, Sitges, June 10-14 (1996) 2008.

[115] Y. Takeuchi et al., Proc. EPAC1996, Sitges, June 10-14 (1996) 2020.

[116] Y. Suetsugu et al., Proc. PAC2003, Portland, May 12?16 (2003) 800.

[117] A. W. Chao and M. Tigner, Handbook of Accelerator Physics and Engineering (World Scientific, 1999) p. 119.

[118] B. Zotter, CERN Report SPS/81-14 (1981).

[119] K-Y. Ng, AIP Conference Proceedings 184, AIP (1989) p.494.